

***Final Draft***  
**of the original manuscript:**

Hegadekatte, V.; Kurzenhaeser, S.; Huber, N.; Kraft, O.:

**A predictive modeling scheme for wear in pin-on-disc and  
twin-disc tribometers**

In: Tribology International (2008) Elsevier

DOI: 10.1016/j.triboint.2008.02.020

Elsevier Editorial System(tm) for Tribology International

Manuscript Draft

Manuscript Number:

Title: A predictive modeling scheme for wear in pin-on-disc and twin-disc tribometers

Article Type: Research Paper

Section/Category:

Keywords: modeling, simulation, finite element method, contact mechanics, ceramics, pin-on-disc, twin-disc

Corresponding Author: Dr. Vishwanath Hegadekatte, Ph.D.

Corresponding Author's Institution: University of Karlsruhe

First Author: Vishwanath Hegadekatte, Ph.D.

Order of Authors: Vishwanath Hegadekatte, Ph.D.; Sven Kurzenhäuser; Norbert Huber, PhD; Oliver Kraft, PhD

Manuscript Region of Origin:

Abstract: Study of sliding and rolling/sliding wear in complex micro-mechanical components is often accomplished experimentally using a pin-on-disc and twin-disc rolling/sliding tribometer respectively (conducted within the parameter space of the tribo-components). The present paper proposes an approach that involves a computationally efficient incremental implementation of Archard's wear model on the global scale (Global Incremental Wear Model - GIWM) for modeling sliding and slipping wear in such experiments. It will be shown that this fast simplistic numerical tool can be used to identify the wear coefficient from pin-on-disc experimental data and also predict the wear depths within a limited range of parameter variation. Further it will also be used to study the effect of introducing friction coefficient into the wear model and also to model water lubricated experiments. A similar tool is presented to model wear due to a defined slip in a twin-

disc rolling/sliding tribometer. The resulting wear depths from this tool is verified using two different finite element based numerical tools namely, the Wear-Processor, which is a FE post processor, and a user-defined subroutine UMESHMOTION in the commercial FE package ABAQUS. It will be shown that the latter two tools have the potential for use in predicting wear and the effective life span of any general tribosystem using the identified wear coefficient from relevant tribometry data.

# A predictive modeling scheme for wear in pin-on-disc and twin-disc tribometers

V. HEGADEKATTE<sup>1\*</sup>, S. KURZENHÄUSER<sup>2</sup>, N. HUBER<sup>3,4</sup>, O. KRAFT<sup>1,5</sup>

<sup>1</sup>Institut für Zuverlässigkeit von Bauteilen und Systemen, Universität Karlsruhe (TH), Kaiserstrasse 12, D-76131, Karlsruhe, Germany.

<sup>2</sup>Institut für Werkstoffkunde II, Universität Karlsruhe (TH), Kaiserstrasse 12, D-76131, Karlsruhe, Germany.

<sup>3</sup>Institut für Werkstoffforschung, GKSS-Forschungszentrum Geesthacht GmbH, Max-Planck-Strasse, D-21502, Geesthacht, Germany.

<sup>4</sup>Institut für Werkstoffphysik und Technologie, Technische Universität Hamburg-Harburg, Eissendorfer Strasse 42(M), D-21073, Hamburg, Germany.

<sup>5</sup>Institut für Materialforschung II, Forschungszentrum Karlsruhe GmbH, Hermann von Helmholtz Platz 1, D-76344, Eggenstein-Leopoldshafen, Germany.

## Abstract

Study of sliding and rolling/sliding wear in complex micro-mechanical components is often accomplished experimentally using a pin-on-disc and twin-disc rolling/sliding tribometer respectively (conducted within the parameter space of the tribo-components). The present paper proposes an approach that involves a computationally efficient incremental implementation of Archard's wear model on the global scale (Global Incremental Wear Model - GIWM) for modeling sliding and slipping wear in such experiments. It will be shown that this fast simplistic numerical tool can be used to identify the wear coefficient from pin-on-disc experimental data and also predict the wear depths within a limited range of parameter variation. Further it will also be used to study the effect of introducing friction coefficient into the wear model and also to model water lubricated experiments. A similar tool is presented to model wear due to a defined slip in a twin-disc rolling/sliding tribometer. The resulting wear depths from this tool is verified using two different finite element based numerical tools namely, the Wear-Processor, which is a FE post processor, and a user-defined subroutine UMESHMOTION in the commercial FE package ABAQUS. It will be shown that the latter two tools have the potential for use in predicting wear and the effective life span of any general tribosystem using the identified wear coefficient from relevant tribometry data.

---

\*Corresponding Address

Institut für Werkstoffphysik und Technologie  
Technische Universität Hamburg-Harburg  
Eissendorfer Strasse 42(M),  
D-21073, Hamburg, Germany  
Tel.: 00 49 40 42878 4386  
Fax: 00 49 40 42878 4070  
E-Mail: hegadekatte@tuhh.de

# 1 Introduction

Of the various reliability issues concerning micro-mechanical components, wear is the least predictable partially due to the imperfect knowledge of the appropriate wear rate for the selected material pair which in turn greatly hinders our ability to predict the effective life span of components. Often, experimental techniques like pin-on-disc, twin-disc, scratch test, AFM etc. are used to characterize the tribological properties of various materials used for fabricating micro-machines in order to reduce the dependence on expensive in-situ wear measurements on prototypes of micro-machines. These experiments attempt to mimic the contact conditions of the tribosystem under study in terms of contact pressure, sliding velocity etc. The specimens should have the same microstructure as the micro-machine itself and the loading chosen in the experiments are such that they mimic the micro-machine. For example, twin-disc rolling/sliding tribometer tries to mimic the rolling/sliding contact experienced by micro-machines e.g., between the teeth of two mating micro-gears. Such experiments allow for a qualitative study of the suitability of a particular material combination for a given application and therefore modeling of wear in such experiments is necessary in order to predict wear in micro-machines itself.

Over the past, modeling of wear has been a subject of extensive research [1] in order to derive predictive governing equations. The modeling of wear found in the literature [2, 3, 4, 5] can broadly be classified into two main categories, namely, (i) mechanistic models, which are based on material failure mechanism e.g., ratchetting theory for wear [6, 7] and (ii) phenomenological models, which often involve quantities that have to be computed using principles of contact mechanics e.g., Archard's wear model [8].

Archard's wear model is a simple phenomenological model, which assumes a linear relationship between the volume of material removed,  $V$ , for a given sliding distance,  $s$ , an applied normal load,  $F_N$  and the hardness (normal load over projected area) of the softer material,  $H$ . A proportionality constant, the wear coefficient,  $k$  characterizes the wear resistance of the material:

$$\frac{V}{s} = k \frac{F_N}{H}. \quad (1)$$

Wherever the conventional Archard's equation did not hold, researchers have modified the model to suit their specific cases. One such example is the modifications of Archard's equation to include wear of highly elastic/pseudo elastic materials in [9]. Sarkar has given an extension to the Archard's wear model that relates the friction coefficient and the volume of material removed [10]:

$$\frac{V}{s} = k \frac{F_N}{H} \sqrt{1 + 3\mu^2} \quad (2)$$

Even though this model was originally introduced to study wear in the presence of asperity junction growth, it will be shown in this article that this model when applied on the global scale can favorably describe the trends observed in the experiments considering the uncertainties in the measurement.

Researchers have used both the above categories of wear models in computer simulation schemes e.g., Ko et al. applied linear elastic fracture mechanics and finite element modeling to predict fatigue wear in steel [11] which basically is based on the idea of a mechanistic wear model (The delimitation theory of wear) proposed by Suh [12, 13]. The ratchetting theory for wear has been used in wear simulation schemes by [14-16]. [17-19] made qualitative prediction of the wear of coated samples in a pin-on-disc tribometer which showed good qualitative agreement with experimental results.

On the other hand, a modification of Archard's phenomenological wear model where the hardness of the softer material was allowed to be a function of temperature was used by Molinari et al. [20] and they also used an elastic-plastic material model for the contacting bodies. Due to the computational expense, only a simple contact problem of a block sliding/oscillating over a disc was simulated. As a faster and efficient approach, post-processing of the finite element contact results with Archard's wear model to compute the progress of wear for a given time interval/sliding distance has started to gain popularity in the recent years as illustrated by the works in [21-28]. [29, 30] have implemented a re-meshing scheme for geometry update in a similar setting. [31-34] have included a three dimensional finite element model and also a re-meshing scheme for simulating wear and have also shown that their results compare favorably with experimental data. The computational costs in such finite element based approaches are mainly from to the computation of the contact stresses, which requires the solution of a nonlinear boundary value problem often using commercial finite element packages.

In case of tribo-systems with simple geometries, especially tribometers e.g., pin-on-disc, twin-disc etc., the estimation of the contact area can be simple. In such cases, it may not be necessary to solve the contact problem using finite elements and instead wear can be modeled on the global scale like in the Global Incremental Wear Model (GIWM) to be presented in the following. The estimation of the contact area in the GIWM is accomplished by considering both the normal elastic displacement and wear which is normal to the contacting surface. From the applied normal load and the estimated contact area, an average contact pressure across the contacting surface is calculated. The average contact pressure (global quantity) is then used in a suitable wear model to calculate the increment of wear depth for a pre-determined sliding distance increment. The wear depth is then integrated over the sliding distance to get the traditional wear depth over sliding distance curves. A detailed explanation on GIWM was presented in [32], where the GIWM was successfully applied to fit and predict predominantly disc wear in a pin-on-disc experiment.

## **2 Global Incremental Wear Model for pin wear in a pin-on-disc tribometer**

The experimental results presented in this work are from unidirectional sliding tests. A micro pin-on-disc tribometer with a spherical tipped pin and a disc of the same material was used in the tests. Two sets of experiments were carried out over a sliding distance of

500 m at room temperature, in ambient air and in water at various normal loads and a sliding speed of 400 mm/s. The ground disc specimens had the dimensions of  $\varnothing 8 \times 1$  mm<sup>2</sup> and the polished pin specimens had a diameter of 1.588 mm. The disc surface had an average surface roughness of  $R_a = 0.11$   $\mu\text{m}$  and for the pin specimens  $R_a = 0.07$   $\mu\text{m}$  for Si<sub>3</sub>N<sub>4</sub> and for WC-Co experiment, the pin and disc had a polished surface with an average surface roughness  $R_a = 0.019$   $\mu\text{m}$  and  $R_a = 0.020$   $\mu\text{m}$  respectively. The parameters used in the experiments were based on a system analysis of a micro-turbine and a -planetary gear train presented in chapter 1 of [35]. The normal force and the friction force were continuously measured with the help of strain gages during the tests. The sum of the wear depth on both the pin and the disc was also continuously measured capacitively within a resolution of  $\pm 1$   $\mu\text{m}$ . In these experiments it was observed that the wear on the disc was below 200 nm for Si<sub>3</sub>N<sub>4</sub>. For the WC-Co experiments, disc wear was not measurable. At the end of the experiment, the maximum wear depth of pin and

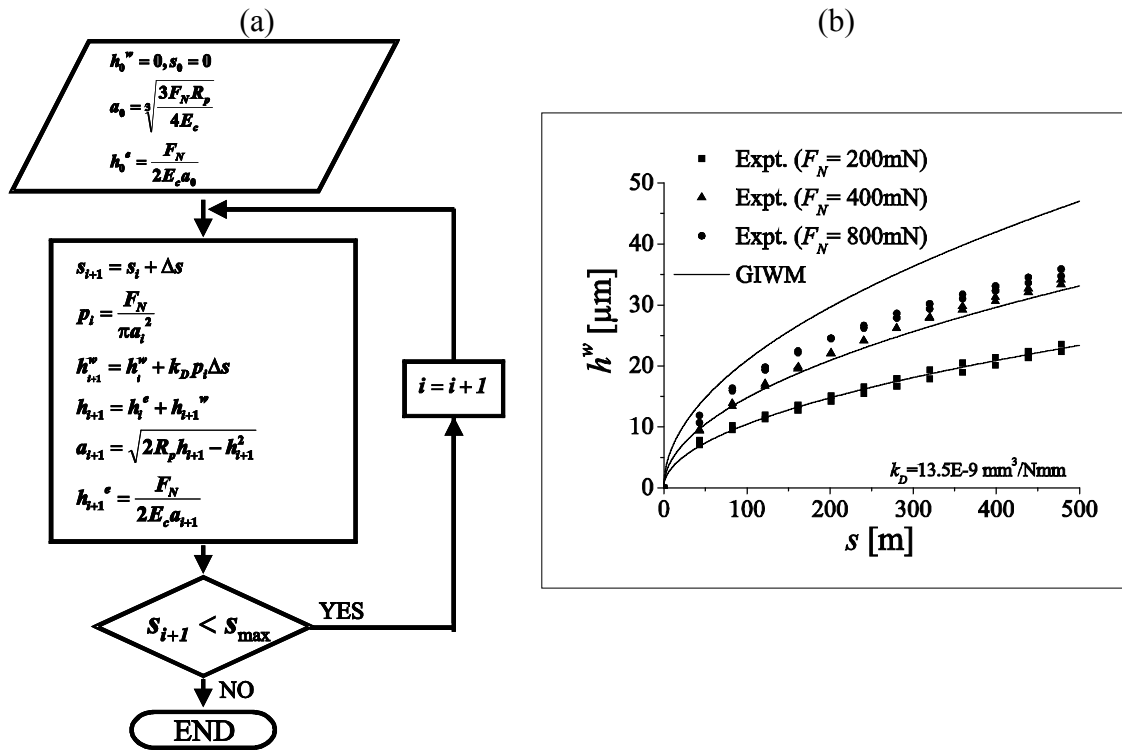


Fig. 1: (a) Flow chart of the Global Incremental Wear Model for pin-on-disc tribometer (b) Results from the GIWM in comparison with the experimental results from the pin-on-disc tribometer at three different normal loads (200 mN, 400 mN and 800 mN)

disc was measured by white-light and contact profilometry respectively. The discrepancy between in-situ measured wear from the capacitive displacement sensor and the wear calculated from the flat circular contact area of the worn pin did not exceed  $\pm 250$  nm for the WC-Co pairing at the end of the experiment. For the simulation, the capacitively measured linear wear was fitted to the values obtained for pin wear at the end of the experiment, assuming a linear drift of the capacitive device. The wear depth data as a function of the sliding distance is shown in Fig. 1 (a) and (b) for Si<sub>3</sub>N<sub>4</sub>.

For the sake of clarity of the present article, the GIWM for pin wear will be explained in the following. The flow chart of this scheme is shown in Fig. 1 (a), where  $p$  is the contact pressure,  $F_N$  is the applied normal load,  $a$  is the contact radius due to elastic displacement and wear,  $h$  is the total displacement at the pin tip,  $R_P$  is the curvature of the pin,  $h^e$  is the elastic displacement,  $h^w$  is the current wear depth,  $k_D = k/H$  is the dimensional wear coefficient,  $\Delta s$  is the interval of the sliding distance,  $s_{max}$  is the maximum sliding distance,  $i$  is the current wear increment number and  $E_C$  is the elastic modulus of the equivalent surface calculated using the following equation (see page 92 of [36]):

$$\frac{1}{E_c} = \frac{1 - \nu_p^2}{E_p} + \frac{1 - \nu_d^2}{E_d} \quad (3)$$

where  $E_p$  and  $E_d$  are the Young's modulus of the pin and disc respectively and the Poisson's ratios of the pin and the disc is represented by  $\nu_p$  and  $\nu_d$  respectively.

The global wear modeling scheme begins with the computation of the initial contact radius  $a_0$  using the Hertz solution [37]

$$a_0 = \sqrt[3]{\frac{3F_N R_P}{4E_C}} \quad (4)$$

and the elastic deformation normal to the contact using the relation found in [38]:

$$h_{i+1}^e = \frac{F_N}{2E_c a_{i+1}} \quad (5)$$

After each increment of sliding distance the current contact radius  $a_i$  is computed from the geometry of the contact based on the sum of the wear depth and the elastic deformation normal to the contact. The wear depth is integrated over the sliding distance using the Euler explicit method:

$$h_{i+1}^w = k_D p_i \Delta s_i + h_i^w \quad (6)$$

till the maximum sliding distance is reached.

## 2.1 Results

### 2.1.1 Application of GIWM to unlubricated pin-on-disc experiment

The GIWM was used to fit the data from the 200 mN normal load experiment (Fig. 1 (b)), where  $k_D$  was identified to be  $13.5 \times 10^{-9} \text{ mm}^3/\text{Nmm}$ . The chosen material properties for silicon nitride were [39]: Young's Modulus,  $E = 304 \times 10^3 \text{ N/mm}^2$  and Poisson's Ratio,  $\nu = 0.24$ . Later, the identified wear coefficient was used to predict the 400 mN and 800 mN experiment.

It can be seen from the graph of the fit for 200 mN and prediction for 400 mN in Fig. 1 (b) that the results from the GIWM are in good agreement with the experiments. However, the GIWM over estimates the wear depth for the 800 mN experiment as shown



in the same figure. As it can be seen from Fig. 1 (b), the wear depth after 500 m of sliding is only slightly higher for 800 mN compared to the 400 mN experiment. One possible reason for this behavior could come from the activation of a different dominant wear mechanism or formation of protective tribological layers reducing the wear rate. Such effects are not included in the Archard's wear model and therefore more experimental data would be needed to extend the Archard's wear model for inclusion in GIWM. However, up to the first 100 m of sliding, the GIWM is still in good agreement for the 800 mN experiment. The GIWM was successful in predicting the results of pin-on-disc experiment when the normal load was doubled.

### 2.1.2 Application of GIWM using Sarkar's wear model

GIWM offers a unique possibility to implement any wear model on the global scale with relative ease. In order to investigate the effect of the changing friction coefficient we use the modified Archard's wear model given by Sarkar (see Equation (2)) to study the evolution of wear depth for the pin in the silicon nitride experiments discussed above. The coefficient of friction,  $\mu$  in Equation (2) was based on an exponential fit as given in Equation (7):

$$\mu = A \cdot e^{-s/c} + b \quad (7)$$

where  $s$  is the sliding distance and  $A$ ,  $b$ ,  $c$  are the parameters defining the change of  $\mu$  with increasing  $s$ . The graph showing the fit and the values for the above parameters from the fit for the 200 mN, 400 mN and 800 mN experiment are given in Fig. 2 (a), (c), (e) and Table 1 respectively.

The GIWM with Sarkar's modified Archard's wear model was used to fit the 200 mN normal load experiment. The identified value of  $k_D$  using was  $10.2 \times 10^{-9} \text{ mm}^3/\text{Nmm}$  which was now slightly lower (approximately by a factor  $\sqrt{1+3\mu^2}$  for  $\mu \sim 0.45$ ) when compared to that identified from the conventional Archard's wear model. However, the resulting curves for the wear depth over sliding distance for the fit (200 mN) was in exact agreement as shown in Fig. 3.

Table 1: Values of the parameters from the exponential fit (Equation 7) of the measured value of the friction coefficient as a function of the sliding distance for different normal loads

Parameter	200 mN	400 mN	800 mN
A	0.226	0.244	0.284
b	0.496	0.396	0.404
c	32.877	607.837	81.704

Fig. 2 (b), (d) and (f) shows  $k_D$  as a function of  $\mu$  calculated from the 200 mN, 400 mN and 800 mN experiments in comparison to that from Sarkar's modified Archard's wear model implemented in GIWM. The effect of introducing friction into the wear model can be clearly seen for the prediction of the 400 mN and 800 mN experiments in Fig. 3. The prediction for 400 mN is an under estimate when compared with the experimental results.

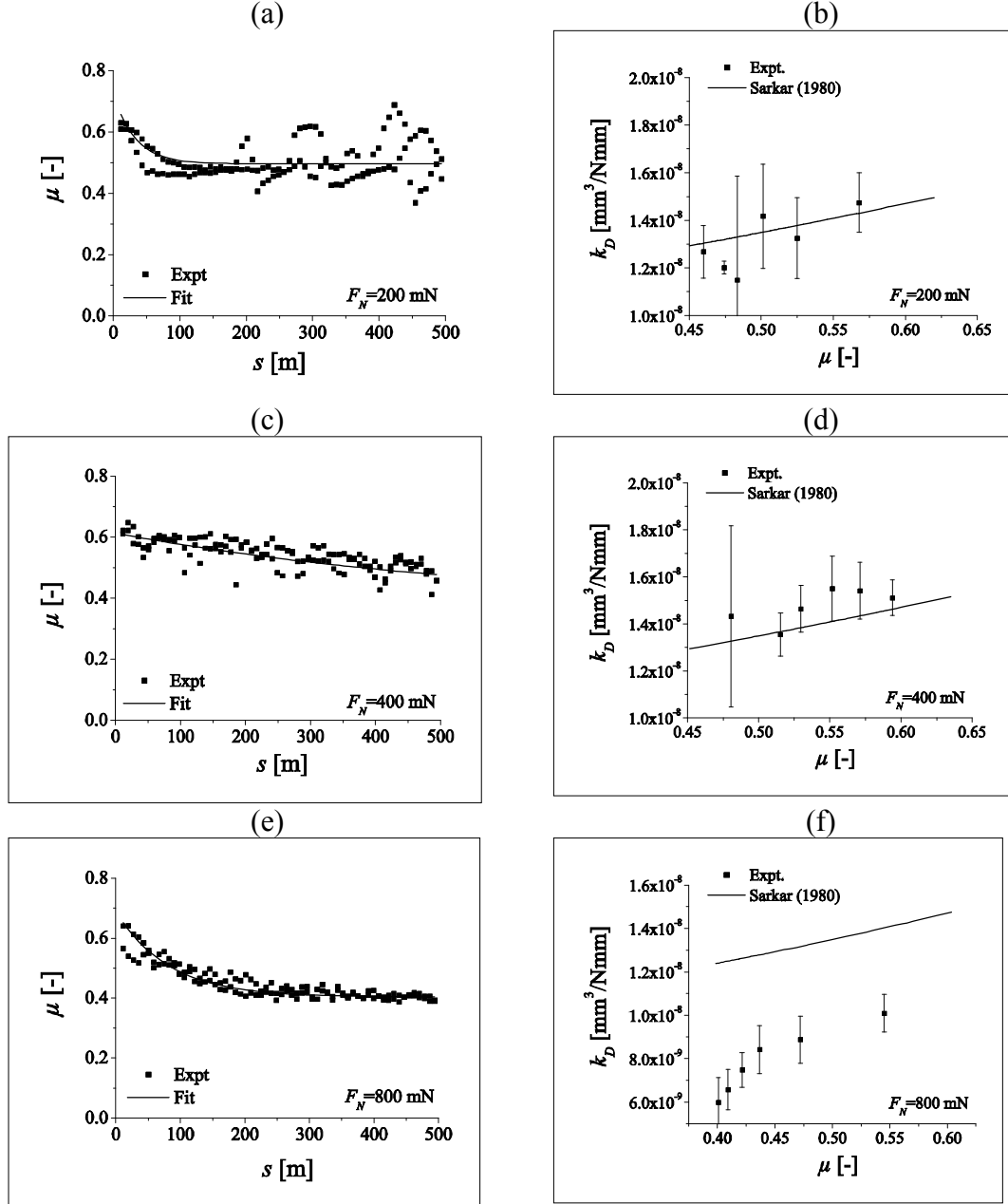


Fig. 2 : Graph showing the exponential fit on the measured  $\mu$  as a function of  $s$  for (a) 200 mN, (c) 400 mN and (e) 800 mN normal load; Comparison of  $k_D$  as a function of  $\mu$  from the experiments on silicon nitride and from the modified wear model of Sarkar with  $k_D = 10.2 \times 10^{-9} \text{ mm}^3/\text{Nmm}$  for (b) 200 mN, (d) 400 mN and (f) 800 mN normal load.

This under estimation becomes clear when Fig. 2 (b) and (d) are compared. It can be seen that for the 400 mN the effective  $k_D$  values (see Equation (2)) are on the lower side of the

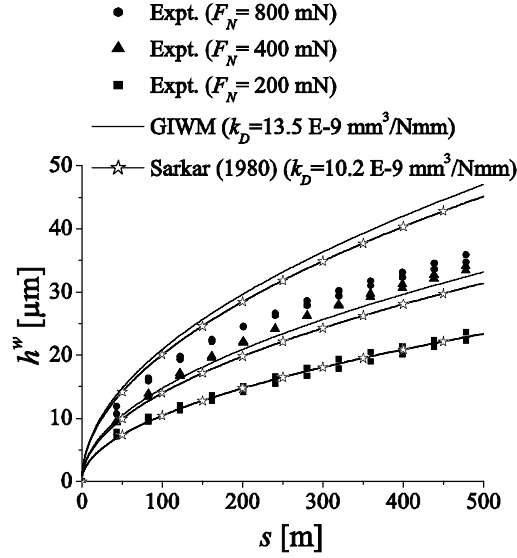


Fig. 3: Results from the Sarkar’s wear model (Equation (2)) implemented within the GIWM for pin wear in comparison with the experimental results from the pin-on-disc tribometer at three different normal loads (200 mN, 400 mN and 800 mN).

corresponding calculated values from the experimental data which is in contrast to the 200 mN experiment. As in the case of Archard’s wear model discussed earlier, the Sarkar’s model still over estimates for the 800 mN experiment. Fig. 3 (f) makes this difference clear as the effective  $k_D$  value is very much higher than that calculated from the experiments. The difference between the curves in Fig. 3 using Archard’s wear model and Sarkar’s model is due to the inclusion of friction into the wear model in the latter. However, it can be concluded from Fig. 3 that the effect of including friction in the wear model has marginal influence on the wear behavior for silicon nitride. However it should be noted that Sarkar’s model can satisfactorily describe the trends in the experiments considering the scatter in the measured data as shown in Fig. 2 (b), (d) and (f).

### 2.1.3 Application of GIWM to water lubricated pin-on-disc experiment

The GIWM was used to fit and predict another set of experiments for the same specimen geometry of the tribometer as explained before but with the materials as tungsten carbide-cobalt and the experiments were water lubricated with all the other parameters remaining the same as described before. Fig. 4 shows the wear depth as a function of the sliding distance for different applied normal loads. The “step” of size approximately 300 nm in the experimental wear depth curve in Fig. 4 is a result of the measurement uncertainty. As stated earlier, the resolution of the tribometer is 1  $\mu\text{m}$  while the maximum wear measured at the highest load is around 2  $\mu\text{m}$ . The wear coefficient,  $k_D$  was identified to be  $0.75 \times 10^{-11} \text{ mm}^3/\text{Nmm}$  from the fit for the 400 mN experiment and was then used to predict the wear depth for higher loads. The material properties used for WC-Co were: Young’s Modulus of the pin,  $E_p = 320 \times 10^3 \text{ N/mm}^2$ , and for the disc,  $E_d = 305 \times 10^3 \text{ N/mm}^2$  and Poisson’s Ratio,  $\nu = 0.24$ . It can be seen in Fig. 4 that the GIWM can predict

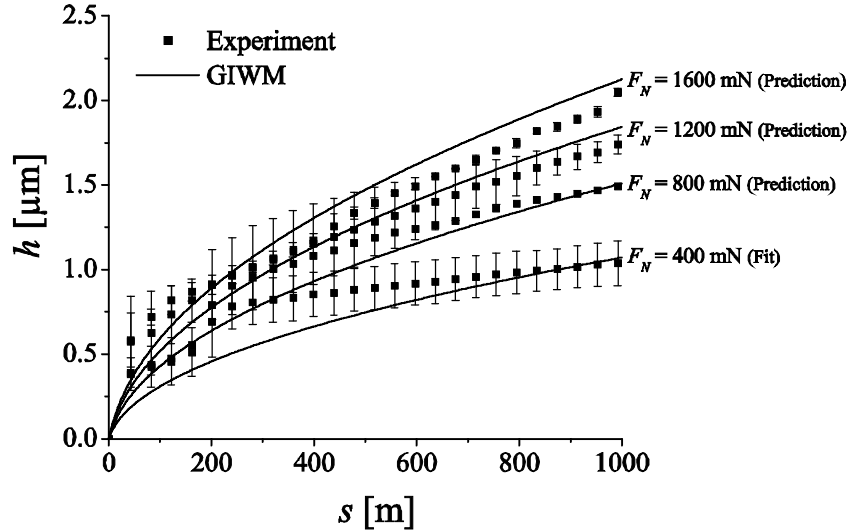


Fig. 4: Wear depth data for pin wear as function of the sliding distance in comparison to the results from the GIWM for different normal loads (400 mN, 800 mN, 1200 mN and 1600 mN). (No Error bars for 800 mN are presented as the discrepancy between continuously measured wear and the wear measured after the experiment exceeded 250 nm in one of the experiments)

the experiments with reasonable accuracy considering the scatter in the measurement for the entire range of normal loads tested. The identified wear coefficient should be construed as a tribosystem dependent quantity which includes all the effects resulting from e.g., lubrication, surface roughness, temperature etc. Thus, we assume that the wear coefficient identified in such a way can be used to predict wear in any general tribosystem as far as the identification of the wear coefficient is done from experiments which are conducted within the parameter space of the tribosystem itself.

### 3 Global Incremental Wear Model for disc wear in a twin-disc tribometer

When two circular rotating bodies (e.g. see Fig. 5 (a)) come in contact with each other and they have the same tangential velocity at all points of contact, then they are said to exhibit pure rolling contact. In pure rolling there will be no slip at the contact interface. However, in reality it is very difficult to find a contact situation that exhibits pure rolling. Local sliding will most likely take place on a part of the contact e.g., in gears, tooth flanks roll and slide against each other at all locations along the tooth flank except at the pitch point [40]. Therefore, most rolling contacts are in essence rolling/sliding contacts. Such contacts are often experimentally studied with twin-disc rolling/sliding tribometer shown in Fig. 5 (a).

The two circles on top disc in Fig. 5 (a) and (b) indicate that the top disc has a curved surface whereas the bottom disc has a flat surface. Such an arrangement helps in better

alignment of the two discs while conducting the experiments. The two discs rotate with velocities  $V_1$ , and  $V_2$  (at the outermost circumference), such that  $V_1 \neq V_2$ . The existence of slip between the discs together with normal load acting on them, results in sliding wear, for which Archard's wear law is known to be applicable. Such a system can be assumed to be like the one shown on the right hand side of Fig. 5 (b), in which the bottom disc is fixed and the top disc rotates at the slip velocity. With this assumption, the problem can be reduced from rolling/sliding contact to quasi-static sliding contact. However, this assumption is valid only when the bottom flat surfaced disc does not wear out at all. Since this assumption is valid in the analysis presented in this paper, the bottom disc is modeled as an analytical rigid surface in the finite element model used by the Wear-Processor and UMESHMOTION.

The increment of wear depth using the Archard's wear model in Equation (6) has to be adopted for the case of twin-disc tribometer. Equation (6) will have to be re-written as in Equation (8), since, as the disc rotates the contact pressure on any surface point approaches to a maximum from zero and then gradually approaches to zero. The point

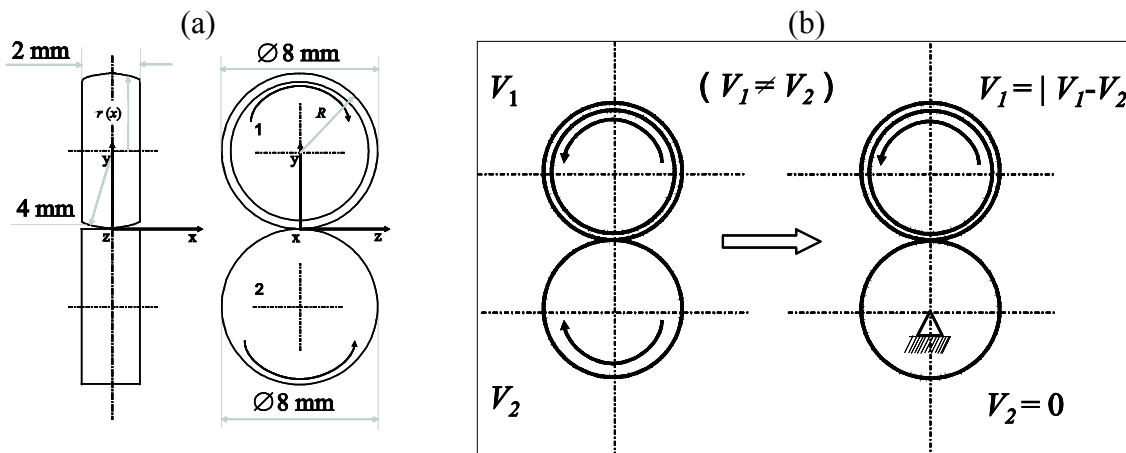


Fig. 5: (a) Schematic of the twin-disc tribometer (shaded portion in the schematic is modeled with FE for use in Wear-Processor and UMESHMOTION), (b) Reduction of rolling/sliding contact with defined slip to sliding contact in the twin-disc tribometer

wears only when it experiences pressure while passing through the contact interface. Therefore, pressure acting on this point, has to be integrated along the sliding direction corresponding to one rotation for the computation of the local wear increment. Therefore, for one rotation of the disc, the wear taking place on this point can be written as:

$$h_{j+1} = k_D \int_{\phi=0}^{\phi=2\pi} p r d\phi + h_j, \quad (8)$$

where  $r = r(x)$  is the radius of the disc at the location of the point (since the top disc surface is curved) and  $\phi$  is the angle of rotation. The calculation of wear depth using Equation (8) will hold for all the nodes lying along the same circumference (streamline). For a given time increment  $\Delta t_j$ , the wear depth can then be written as:

$$h_{j+1} = k_D \frac{\Delta t_j |V_1 - V_2|}{2\pi r} \int_{\phi=0}^{\phi=2\pi} p r d\phi + h_j. \quad (9)$$

In this local form of the Archard's wear model the contact pressure,  $p$  is different for each streamline which is inherently considered in finite element based wear simulation tools

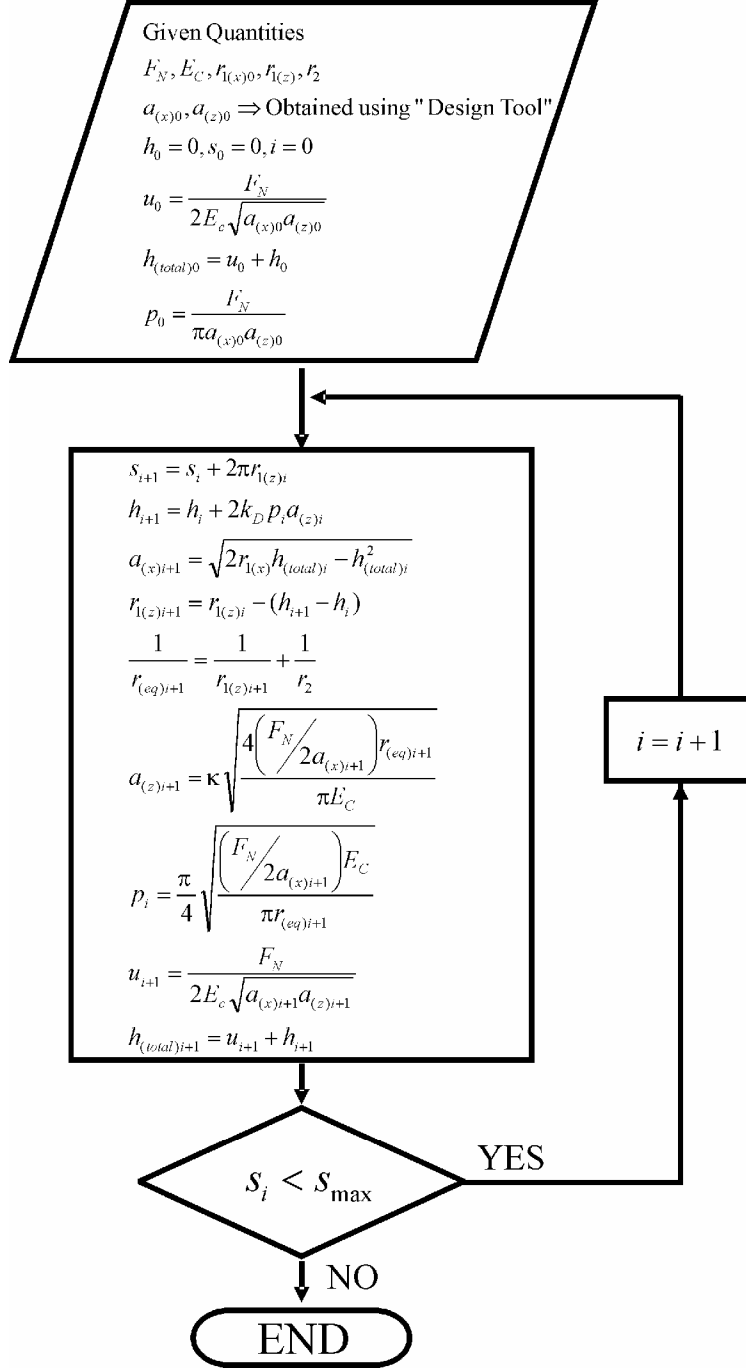


Fig. 6: Flow chart of the Global Incremental Wear Model for twin-disc rolling/sliding tribometer

such as the Wear-Processor [31, 32] or UMESHMOTION. The latter is a user defined

subroutine in the commercial finite element package ABAQUS to be discussed in the following.

For the GIWM as the word “global” suggests and as discussed in the previous section, an average contact pressure over the entire contact area is assumed. Further, it is assumed that the bottom flat surfaced disc is rigid and therefore all the wear occurs on the top curved surfaced disc while negligible wear occurs on the bottom disc. Therefore the top disc is assumed to have an elastic modulus equal to the contact modulus (see Equation (3)). The contact area in such a contact is elliptical. The major axis of the contact ellipse will be perpendicular to the direction of rotation and the minor axis will be tangential to the direction of rotation of the discs. The flow chart of the GIWM for disc wear in a twin disc rolling/sliding tribometer is shown in Fig. 6, where  $p$  is the average contact pressure,  $F_N$  is the applied normal load,  $a_{(x)}$  is the semi major axis length of the contact ellipse (perpendicular to the direction of rotation) and  $a_{(z)}$  is the semi minor axis length of the contact ellipse (tangential to the direction of rotation),  $h$  is the wear depth,  $r_{1(x)}$  and  $r_{1(z)}$  are the radius of curvature of the top disc and  $r_2$  is the radius of curvature of the bottom disc,  $\kappa$  is the correction factor for  $a_{(x)}$  (to be explained in the following),  $u$  is the elastic displacement,  $h_{(total)}$  is the total displacement of the top disc which is the sum of wear depth and elastic deformation,  $k_D = k/H$  is the dimensional wear coefficient,  $s$  is the sliding distance,  $s_{max}$  is the maximum sliding distance,  $i$  is the current wear increment number and  $E_C$  is the elastic modulus of the equivalent surface (see Equation (3)).

The global wear modeling scheme begins with the computation of the initial semi axis lengths of the contact ellipse using the Hertz solution [37] for elliptical contact area and the initial normal elastic deformation using the relation found in [38] which is corrected for the elliptical contact area:

$$u_0 = \frac{F_N}{2E_c \sqrt{a_{(x)0} a_{(z)0}}} \quad (10)$$

Then, the initial average contact pressure,  $p$  over the elliptical contact area and the total displacement,  $h_{(total)}$  of the disc surface is calculated. The wear depth is integrated over the sliding distance,  $2a_{(z)}$  using the Euler explicit method:

$$h_{i+1} = h_i + 2k_D p_i a_{(z)i} \quad (11)$$

For one rotation of the disc, the sliding distance increment over which wear takes place is given by the minor axis length of the contact ellipse,  $2a_{(z)}$ . The current semi major axis length of the contact ellipse,  $a_{(x)}$  and the radius of the top disc,  $r_{(x)}$  are calculated from the geometry of the contact which changes due to wear. The semi minor axis length of the contact ellipse,  $a_{(z)}$  and the average contact pressure,  $p$  is computed using the Hertz solution [37] for rectangular contact area (assuming a plain strain condition at the center of the contact along the width of the discs) using:

$$a_{(z)i+1} = \kappa \sqrt{\frac{4 \left( \frac{F_N}{2a_{(x)i+1}} \right) r_{(eq)i+1}}{\pi E_C}} \quad (12)$$

and

$$p_i = \frac{\pi}{4} \sqrt{\frac{\left(\frac{F_N}{2a_{(x)i+1}}\right) E_c}{\pi r_{(eq)i+1}}} \quad (13)$$

respectively.

Since an elliptical contact area results from the contact in the twin-disc tribometer and a rectangular contact area is assumed in Equation (12), it needs to be corrected by equating it to the elliptical contact area. Hence, a correction factor of  $\kappa = \pi/4$  is used in Equation (12). The updating of all the parameters and the integration of the wear increment over the sliding distance is continued till a defined maximum sliding distance is reached. In the absence of reliable experimental data for validating the GIWM, in section 3.3 the validation will be carried out using two separate finite element based wear simulation tools.

### 3.1 Wear-Processor

The first of the finite element based wear simulation tools, the Wear-Processor will only be described in brief here for the sake of condensing the present article. It has been described in detail in [31, 32]. The processing of wear begins with the solution of a 3D static contact analysis with infinitesimal rotation of the bottom rigid flat surfaced disc to include the asymmetric effects coming from the friction between the two slipping discs (see Fig. 5 (a) and (b)). The solution of this boundary value problem is accomplished with the commercial finite element code ABAQUS. One quarter of the top curved surfaced disc is modeled with finite element making use of the symmetry and the other disc is modeled as an analytical rigid surface. The stress field, the displacement field and the element topology are then extracted from the finite element results file.

The unit inward surface normal vector at each of the surface nodes is computed based on the element topology by taking the cross product of the four edge vectors that are connected to each of the surface nodes. The contact pressure for each of the surface nodes on the top disc surface is calculated using the extracted stress field and the calculated normal vector. An explicit Euler method is used to integrate Archard's wear law for each surface node over the sliding distance using Equation (9).

The calculated wear from Archard's wear model is used to update the geometry by repositioning the surface nodes with an efficient re-meshing technique that makes use of the boundary displacement method, see [31, 32] for more details. The obtained new reference geometry is used to get the updated stress distribution by solving the contact problem again, which in turn is used to compute the updated contact pressure distribution. At the end of each wear increment, the total displacement (sum of the elastic displacement and wear depth) for each of the surface nodes is written to an ABAQUS compatible file for viewing with PATRAN (a commercial pre- and post-processor). The procedure is continued till a pre defined maximum sliding distance is reached.



It is to be noted that the finite element model used in the wear simulation with the Wear-Processor and the UMESHMOTION was identical. The deformable top curved surfaced disc is not rotated physically in the contact simulation, but it is assumed to be rotated for certain time increment in UMESHMOTION and the Wear-Processor. During this time increment, it is assumed that the configuration changes are negligible and have minor effect on the contact solution.

## **3.2 UMESHMOTION**

The second finite element based wear simulation tool to be discussed in this article is the UMESHMOTION, which is a user-defined subroutine in the commercial FE code ABAQUS. It is intended for defining the motion of nodes in an adaptive mesh constraint node set. By defining the contact surface nodes in the adaptive mesh constraint node set, UMESHMOTION can be coded to shift the surface nodes in the direction of the local normal by an amount equal to the corresponding local wear. In this work, it has been specially coded in FORTRAN to simulate wear in a twin-disc tribometer. A detailed description of the adaptation of UMESHMOTION for simulating wear can be found in [41, 42].

Once the equilibrium equations for the three dimensional, deformable-rigid contact problem converge, the user-defined subroutine UMESHMOTION is called for each surface node. The UMESHMOTION, which is specially coded to simulate wear feeds back the local wear increment for a given time increment calculated using Equation (9). The adaptive meshing algorithm of ABAQUS applies the local wear increment for all surface nodes in two steps. First, the surface nodes are swept in the local normal direction by an amount equal to the corresponding local wear increment. The sweeping of the nodes is carried out purely as an Eulerian analysis. Thus the geometry is updated. Second, the material quantities are re-mapped to the new positions. This is accomplished by advecting the material quantities from the old location to the new location by solving advection equations using a second order numerical method, called the Lax-Wendroff method. The sweeping of the mesh and the advection of the material quantities cause an equilibrium loss. The equilibrium loss is corrected by solving the last time increment of the contact problem [44]. In this way, the contact pressure is updated. The procedure is repeated till a pre defined maximum sliding distance is reached.

## **3.3 Results**

The results from the GIWM are compared with that from the Wear-Processor and the UMESHMOTION discussed above. The parameters used in the wear simulations are given in Table 2.

Table 2: Parameters used for the wear simulation using Wear-Processor and UMESHMOTION

Parameter	Value
Material	ZrO <sub>2</sub>
Young's Modulus	$E_t = E_b = 152$ GPa
Poisson's Ratio	$\nu_t = \nu_b = 0.32$
Applied Normal Load	$F_N = 0.3$ N
Friction Coefficient	$\mu = 0.6$
Dimensional Wear Coefficient	$k_D = 1 \times 10^{-10}$ mm <sup>3</sup> /Nmm
Slip	10 %

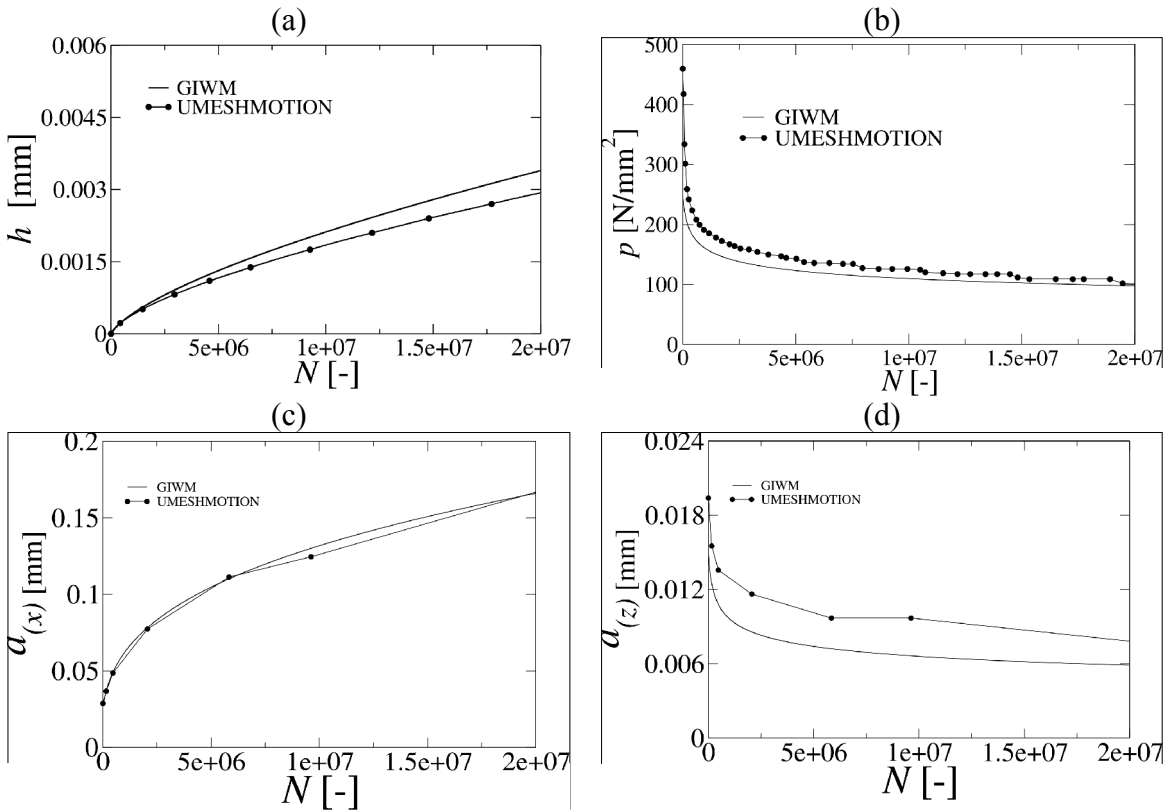


Fig. 7: (a) Graph of wear depth over the number of rotations and (b) graph of the pressure drop over number of rotations using UMESHMOTION and GIWM. (c) Graph showing the semi major axis length and (d) semi minor axis length of the contact ellipse as a function of the number of rotations using UMESHMOTION and GIWM.

The value of the wear coefficient was chosen from pin-on-disc experiments for ZrO<sub>2</sub> from [43]. The results from this wear simulation are presented in Fig. 7 (a) to (d). It can be seen in Fig. 7 (a) that the wear depth as a function of the number of rotations from the GIWM are in good agreement with that from UMESHMOTION (within 16 %). As wear progresses, the curved surface of the top disc progressively flattens leading to a drop in the slope of the wear depth curve because of a drop in the contact pressure (see Fig. 7 (b)) resulting from the increase in the contact area. Due to the flattening of the top disc, the

semi major axis length of the contact ellipse continuously increases (see Fig. 7 (c)) while, the semi minor axis length of the contact ellipse continuously decreases (see Fig. 7 (d)) but the resulting contact area increases.

However, the wear depth curve from the UMESHMOTION in Fig. 7 (a) has a decreasing slope (for larger sliding distances) than that from GIWM. Further the curve from UMESHMOTION lies below that from GIWM which is difficult to explain especially considering the fact that GIWM uses an average pressure for the computation of the wear depth and UMESHMOTION uses the local pressure to compute local wear (see Fig. 7 (b)) which is as high as 1.5 times the average pressure at the contact center. It means that the wear depth curve obtained from the GIWM forms a lower limit for wear depth curves obtained from finite element based wear simulation tools for a given set of initial parameters. To look further into this issue, the wear depth results from the UMESHMOTION was compared with that from the Wear-Processor. The simulations were performed on the same geometry as shown in Fig. 5, but with a coarser mesh (5256 elements compared to 28648 elements) and therefore with a two order of magnitude higher applied normal load and wear coefficient. The coarsely meshed model was used in order to reduce the computation time for performing this study. The wear simulation results using the Wear-Processor, UMESHMOTION and GIWM are shown in Fig. 8. The wear depth curve from the Wear-Processor and the UMESHMOTION will have the same initial slope since they start with the same contact pressure (Hertzian) but the curve from GIWM will have a lower starting slope since it uses an average contact pressure for the computation of wear as can be seen in Fig. 8. As wear progresses, the curves from the Wear-Processor and the GIWM will begin to have the same slope and the accumulated deviation in the early part of sliding remains constant with further increase in the sliding distance. However, it can also be seen in Fig. 8 that the slope of the wear depth curve obtained from the UMESHMOTION continuously decreases as the sliding progresses and shows a trend that it would approach the GIWM curve (also see Fig. 7 (a)). The reason for this discrepancy is not clear. It can be due to either geometry or pressure not being updated correctly or a combination of both. The difference between the wear depth

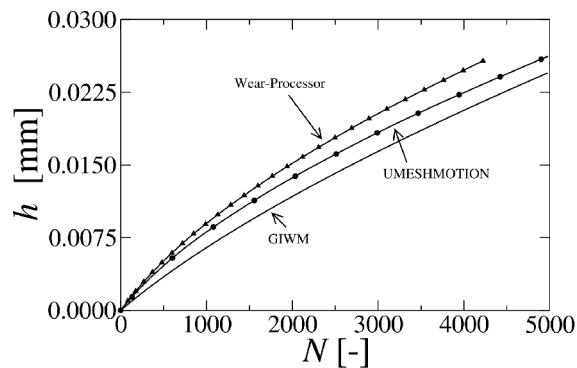


Fig. 8: Graph of wear depth as a function the number of rotations from the Wear-Processor, the UMESHMOTION and the GIWM

obtained from the Wear-Processor and that from the UMESHMOTION is approximately 11 % (within the sliding distance range tested) and seems to be further widening.

It should be noted at this point that while using UMESHMOTION, ABAQUS does not solve the complete contact problem to update the contact pressure distribution, but it only solves the last time increment. The result of this approach is that there is a considerable saving in computational time of the order of one magnitude compared to the Wear-Processor. An additional test was carried out to check if ABAQUS correctly updates the contact pressure distribution. The wear simulation using the UMESHMOTION was interrupted after 2034 rotations and depending on the wear depth distribution at that instance, the geometry was updated externally by repositioning the surface nodes using the boundary displacement method (see [37, 38] for more details). With the resulting new reference geometry the wear simulation using the UMESHMOTION was resumed. If the geometry/pressure was updated correctly, then the resulting pressure distribution on resumption of the wear simulation should exactly be the same as the pressure distribution obtained without any form of external geometry correction. But, it can be seen from Fig. 9 (a) that the pressure updated by ABAQUS does not completely agree with the corresponding pressure at the same location and at the same instance obtained when no external geometry update was applied. The difference is around 7 %.

The effect of this difference can be seen on the wear depth curve shown in Fig. 9 (b). For comparison, the corresponding curves from the Wear-Processor are also presented in the same graph. However, it should be noted that the curve for the pressure drop as a function of the number of rotations is history dependent and since the curve for the pressure drop from the Wear-Processor is obtained by making a “true” update of the geometry, the curves from the UMESHMOTION and Wear-Processor cannot be truly compared. But, as seen from Fig. 9 (b), if the geometry is externally updated, the wear depth curves tend to approach the curve from the Wear-Processor. Thus a frequent external update of the geometry would minimize, the difference between the results from the UMESHMOTION and the Wear-Processor.

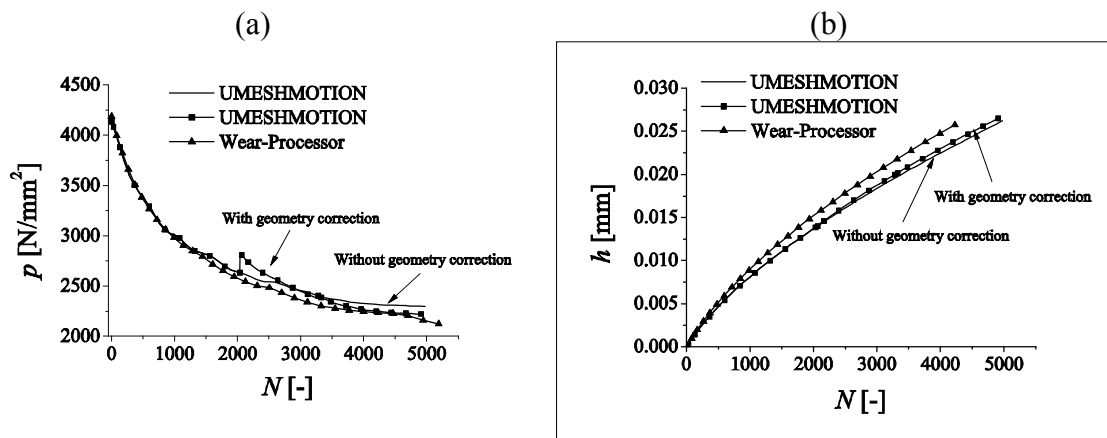


Fig. 9: (a) Graph of pressure drop and (b) wear depth as a function of the number of rotations with and without geometry correction in comparison with the Wear-Processor

The features of the Wear-Processor and the UMESHMOTION include the application of a wear model on the local scale, their ability to simulate wear on three dimensional FE models and their scope for handling arbitrary geometry of tribosystems that could be

made of different materials. However, the Wear-Processor is computationally expensive and therefore has to be used only when it is absolutely necessary for satisfactorily describing the evolution of the worn surface. UMESHMOTION, which is computationally less expensive, can be used in situations where it is sufficient to simulate only one of the contacting surfaces since the contact results are available for only one of the surfaces in this case. This requires, that in the experiments the wear on one of the surfaces is truly negligible.

## **4 Conclusions**

In this work, the Global Incremental Wear Model, which represents a computationally efficient incremental implementation of a suitable wear model on the global scale for modeling sliding and slipping wear, was presented. This fast simplistic numerical tool was used to identify the wear coefficient from pin-on-disc experimental data and also to predict the wear depths within a given range of parameter variation. The results from the GIWM using the Archard's wear model showed a good agreement with the experimental data considering the uncertainties in the measurement. Therefore it can be concluded that Archard's wear model is valid for the materials and the parameters presented in this work including the case when the tribometer is lubricated with water. An extension of the Archard's wear model given by Sarkar was used to study the effect of introducing the friction coefficient into the wear model. This model favorably described the trends seen in the experiments. This tool was further extended to model wear due to a defined slip in a twin-disc rolling/sliding tribometer. The wear depths from this tool was verified using two different finite element based numerical tools namely, the Wear-Processor, which is a FE post processor and the second tool is a user-defined subroutine UMESHMOTION in the commercial finite element package ABAQUS. It was shown that the wear depth results from the GIWM compared favorably with that from the other two numerical tools, thus verifying each other. The difference in the wear depth results from the three numerical tools was within 16 %. Tests on UMESHMOTION showed that there was some discrepancy (of approximately 11 %) in the results when compared to that from the Wear-Processor. Considering the typically larger uncertainties in tribo experiments, the accuracies are acceptable

GIWM assumes a constant average pressure over the contact area in any sliding distance increment. The worn out surface is assumed to be always flat so that the contact area can be easily estimated. These assumptions in the GIWM limit its usage to certain geometries. The GIWM can be used to make a first guess for the local wear model, which can then be implemented in FE based wear simulation tools. This efficient method of wear simulation can be very handy for tribologists to quickly interpret their measured data for most material combinations encountered in practical applications. In the next step, the Wear Processor will be extended towards the wear simulation in transient 2D contact problems that are typical for a micro planetary gear train made of ceramics using wear coefficients identified from pin-on-disc and twin-disc experiments.

## Acknowledgement

The authors would like to thank the German Research Foundation (DFG) for funding this work under sub project D4 within the scope of the collaborative research center, SFB 499 – Design, production and quality assurance of molded microparts constructed from metals and ceramics. The authors would also like to thank Prof. S. Andersson of the Royal Institute of Technology (KTH), Sweden for co-supervising the master thesis of B. Kanavalli.

## References

- [1] Zum-Gahr, K. H. (1987). *Microstructure and wear of materials*. Elsevier, Amsterdam, The Netherlands.
- [2] Meng, H. C. (1994). *Wear modeling: evaluation and categorization of wear models*. PhD thesis, University of Michigan, Ann Arbor, MI, USA.
- [3] Meng, H. C. & Ludema, K. C. (1995). Wear models and predictive equations: their form and content. *Wear*, 181-183, 443-457.
- [4] Hsu, S. M., Shen, M. C., & Ruff, A. W. (1997). Wear prediction for metals. *Tribol. Int.*, 30, 377-383.
- [5] Blau, P. J. (1997). Fifty years of research on the wear of metals. *Tribol. Int.*, 30, 32-331.
- [6] Kapoor, A. & Johnson, K. L. (1994). Plastic ratcheting as a mechanism of metallic wear. *Proc. Roy. Soc. Lon. A*, 445, 367-381.
- [7] Kapoor, A. (1997). Wear by plastic ratcheting. *Wear*, 212, 119-130.
- [8] Archard, J. F. (1953). Contact and rubbing of flat surfaces. *J. Appl. Phys.*, 24, 981-988.
- [9] Liu, R. & Li, D. Y. (2001). Modification of Archard's equation by taking account of elastic/pseudoelastic properties of materials. *Wear*, 251, 956-964.
- [10] Sarkar, A. D. (1980). *Friction and wear*. Academic Press, London.
- [11] Ko, P.L., Iyer, S.S., Vaughan, H., Gadala, M. (2001). Finite element modelling of crack growth and wear particle formation in sliding contact. *Wear*, 251, 1265–1278
- [12] Suh, N. P. (1973). The delamination theory of wear. *Wear*, 25, 111-124.
- [13] Suh, N. P. (1977). An overview of the delamination theory of wear. *Wear*, 44, 1-16.
- [14] Franklin, F. J., Widiyarta, I., & Kapoor, A. (2001). Computer simulation of wear and rolling contact fatigue. *Wear*, 251, 949-955.
- [15] Franklin, F. J., Weeda, G.-J., Kapoor, A., & Hiensch, E.J.M. (2005). Rolling contact fatigue and wear behaviour of the infrastar two-material rail. *Wear*, 258, 1048-1054.
- [16] Stalin-Muller, N. & Dang, K. V. (1997). Numerical simulation of the sliding wear test in relation to material properties. *Wear*, 203-204, 180-186.
- [17] Christofides, C., McHugh, P. E., Forn, A., & Picas, J. A. (2002). Wear of a thin surface coating: Modeling and experimental investigations. *Comput. Mat. Sci.*, 25, 61-72.
- [18] Yan, W., Busso, E. P., & O'Dowd, N. P. (2001). A micromechanics investigation of sliding wear in coated components. *Proc. Roy. Soc. Lon. A*, 456, 2387{2407.
- [19] Yan, W., O'Dowd, N. P., & Busso, E. P. (2002). Numerical study of sliding wear caused by a loaded pin on a rotating disc. *J. Mech. Phys. Sol.*, 50, 449-470.
- [20] Molinari, J. F., Ortiz, M., Radovitzky, R., & Repetto, E. A. (2001). Finite element modeling of dry sliding wear in metals. *Engg. Comput.*, 18, 592-609.
- [21] Podra, P. (1997). *FE Wear Simulation of Sliding Contacts*. PhD thesis, Royal Institute of Technology (KTH), Stockholm, Sweden.
- [22] Podra, P. & Andersson, S. (1999). Simulating sliding wear with finite element method. *Tribol. Int.*, 32, 71-81.
- [23] Öquist, M. (2001). Numerical simulations of mild wear using updated geometry with different step size approaches. *Wear*, 249, 6-11.
- [24] Ko, D. C., Kim, D. H., & Kim, B. M. (2002). Finite element analysis for the wear of Ti-N coated punch in the piercing process. *Wear*, 252, 859-869.

- [25] McColl, I. R., Ding, J., & Leen, S. (2004). Finite element simulation and experimental validation of fretting wear. *Wear*, 256, 1114-1127.
- [26] Ding, J., Leen, S. B., & McColl, I. (2004). The effect of slip regime on fretting wear-induced stress evolution. *Int. J. Fatigue*, 26, 521-531.
- [27] Gonzalez, C., Martin, A., Garrido, M. A., Gomez, M. T., Rico, A., & Rodriguez, J. (2005). Numerical analysis of pin on disc tests on Al-Li/SiC composites. *Wear*, 259, 609-612.
- [28] Kónya, L., Váradi, K., & Friedrich, K. (2005). Finite element modeling of wear process of a peek-steel sliding pair at elevated temperature. *Periodica Polytechnica, Mechanical Engineering*, 49, 25 - 38.
- [29] Sui, H., Pohl, H., Schomburg, U., Upper, G., & Heine, S. (1999). Wear and friction of PTFE seals. *Wear*, 224, 175-182.
- [30] Hoffmann, H., Hwang, C., & Ersoy, K. (2005). Advanced wear simulation in sheet metal forming. *Annals of the CIRP*, 54, 217-220.
- [31] Hegadekatte, V., Huber, N., & Kraft, O. (2005). Finite element based simulation of dry sliding wear. *Modelling Simul. Mater. Sci. Eng.*, 13, 57-75.
- [32] Hegadekatte, V., Huber, N., & Kraft, O. (2006). Finite element based simulation of dry sliding wear. *Tribology Letters*, 24, 51-60.
- [33] Kim, N. H., Won, D., Burris, D., Holtkamp, B., Gessel, G., Swanson, P., & Sawyer, W. G. (2005). Finite element analysis and experiments of metal/metal wear in oscillatory contacts. *Wear*, 258, 1787-1793.
- [34] Wu, J. S., Hung, J., Shu, C., Chen, J. (2003). The computer simulation of wear behavior appearing in total hip prosthesis. *Computer Methods and Programs in Biomedicine*, 70, 81-91.
- [35] Eds.: Löhe, D., Haußelt, J. H. (2005). *Micro-Engineering of Metals and Ceramics, Part I and Part II*. Wiley-VCH Verlag GmbH, Weinheim, Germany.
- [36] Johnson, K. L. (1985). *Contact Mechanics*. Cambridge University Press, Cambridge, UK.
- [37] Hertz, H. (1882). Ueber die beruehrung fester elastischer koerper. *J. Reine und Angewandte Mathematik*, 92, 156-171.
- [38] Oliver, W. C. & Pharr, G. M. (1992). An improved technique for determining hardness and elastic modulus using load and displacement sensing indentation experiments. *J. Mat. Res.*, 7, 1564-1583.
- [39] Callister, W. D. (1994). *Material Science and Engineering - An Introduction*. John Wiley and Sons, Inc., New York, USA.
- [40] Flodin, A. & Andersson, S. (1997). Simulation of mild wear in spur gears. *Wear*, 207, 16-23.
- [41] Kanavalli, B. (2006). Application of user defined subroutine UMESHMOTION in ABAQUS to simulate dry rolling/sliding wear. Master thesis, Royal Institute of Technology (KTH), Stockholm, Sweden.
- [42] ABAQUS/Standard 6.5 Example Problems Manual, (Hibbit, Karlsson, & Sorensen, Inc., USA, 2003) 3.1.8.
- [43] Herz, J., Schneider, J., & Zum-Gahr, K. H. (2004). Tribologische charakterisierung von werkstoffen für mikrotechnische anwendungen. In R. W. Schmitt (Ed.), *GFT Tribologie-Fachtagung 2004* Göttingen, Germany. on CD.

Figure 1a

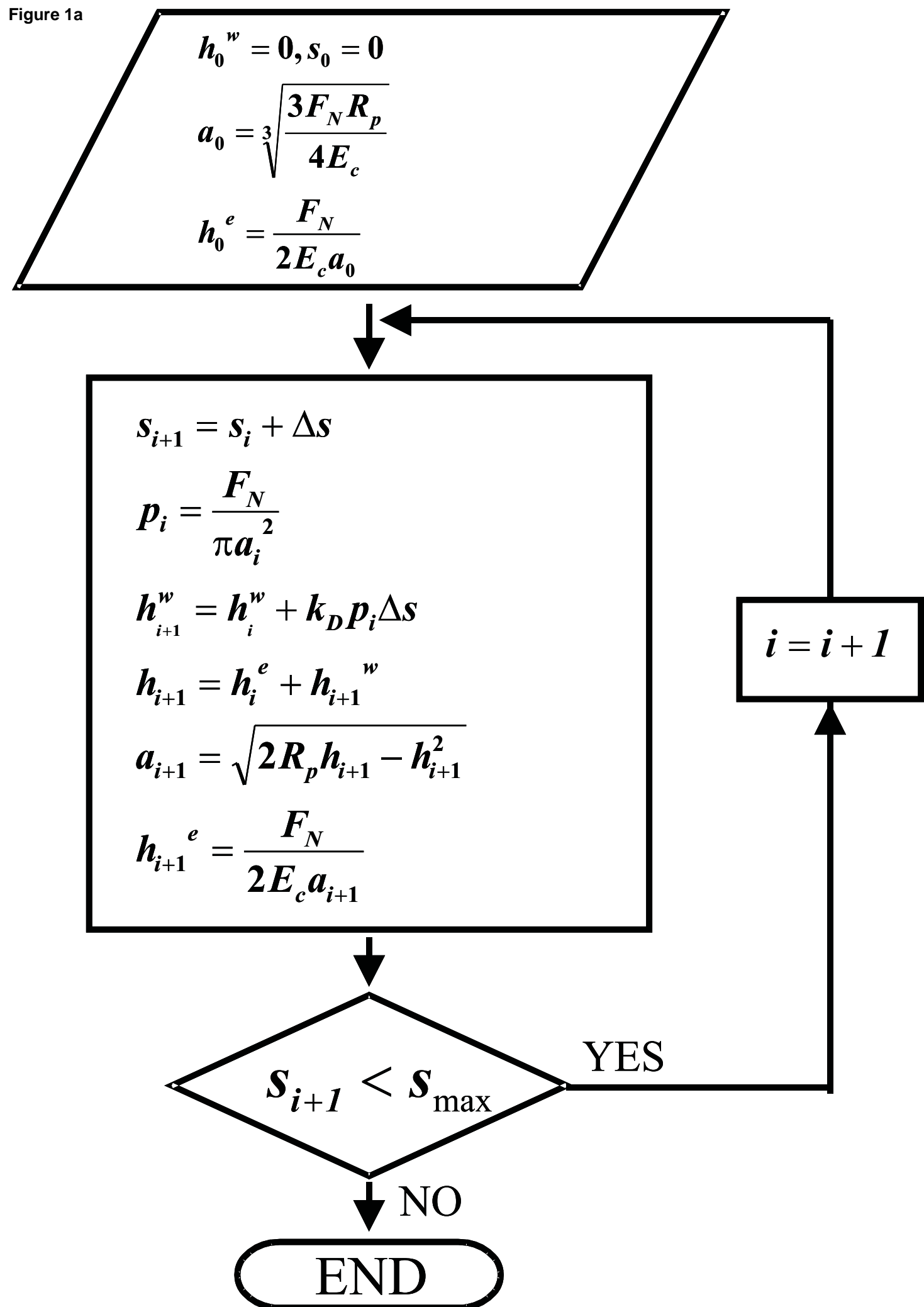




Figure 1b

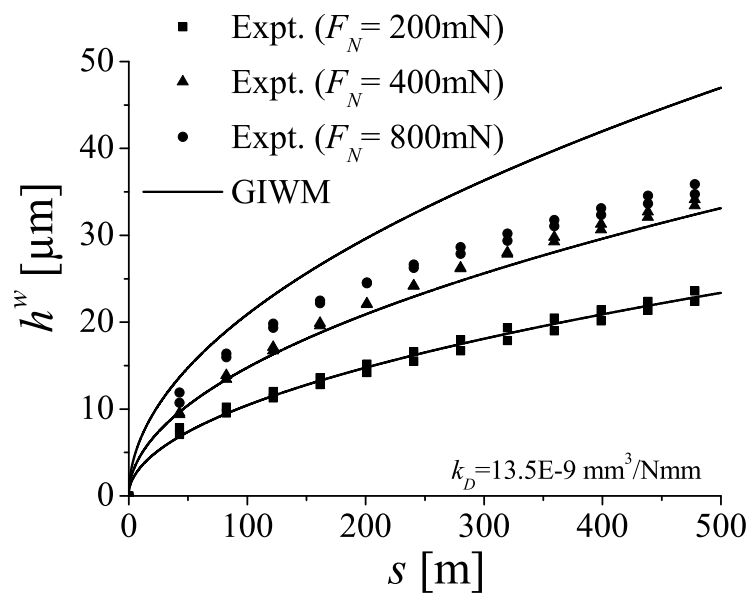


Figure 2a

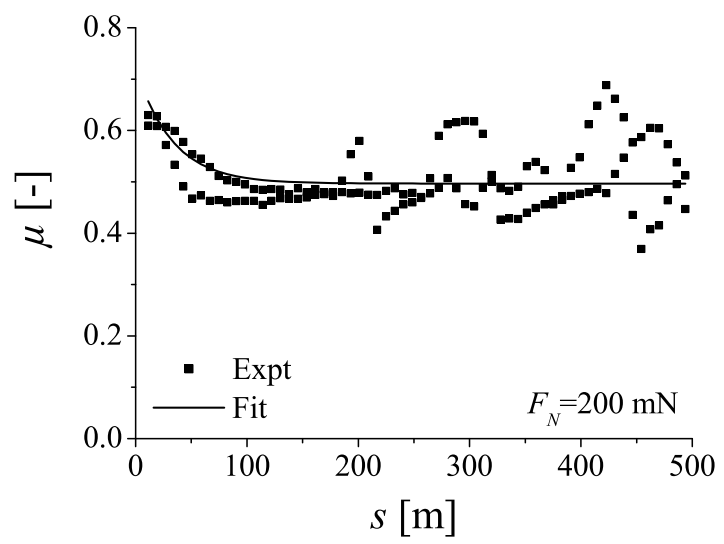


Figure 2b

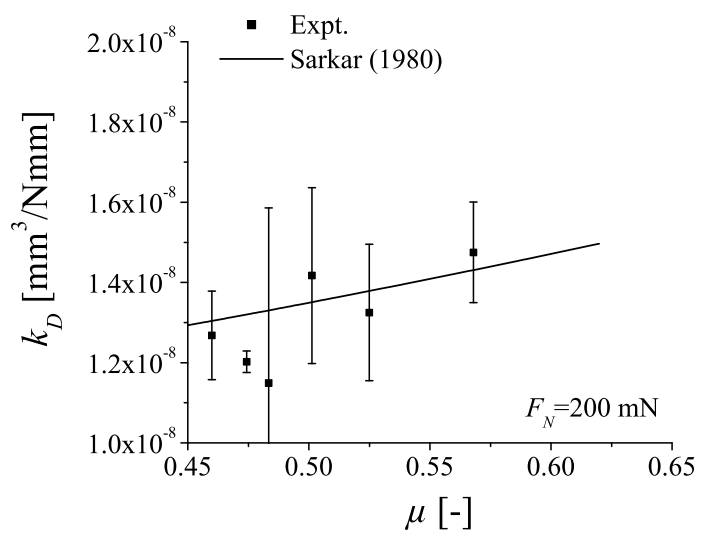


Figure 2c

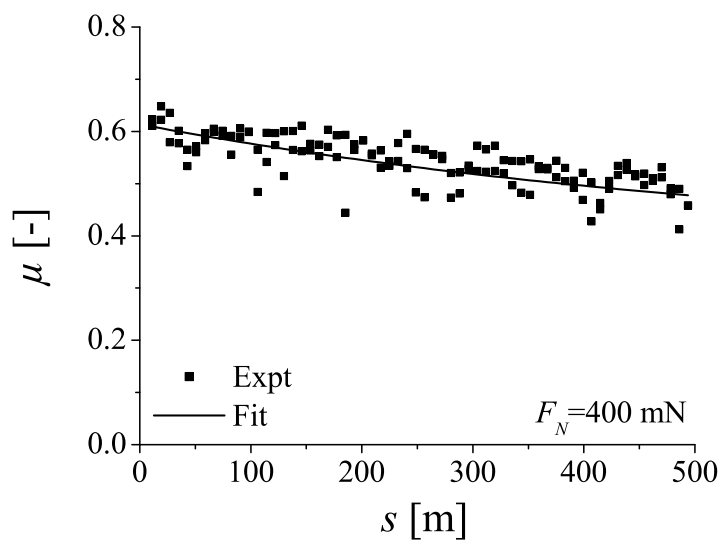


Figure 2d

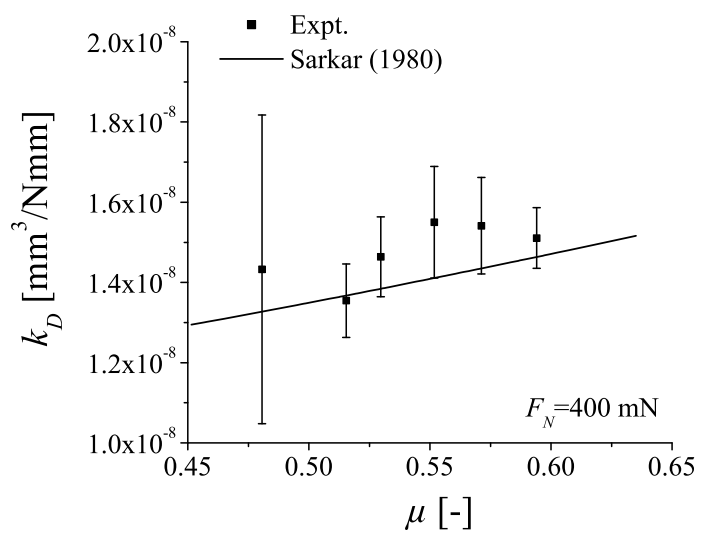


Figure 2e

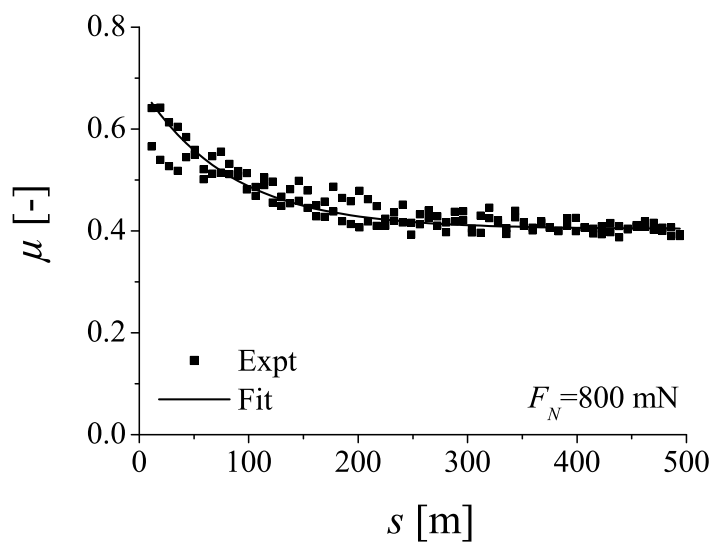


Figure 2f

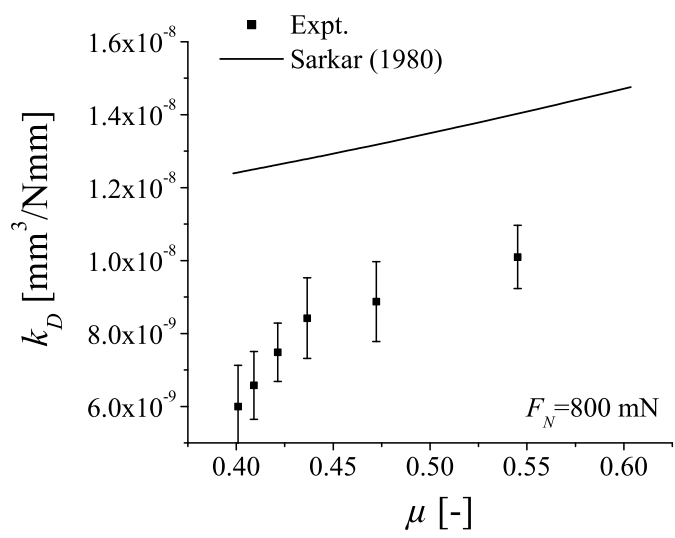


Figure 3

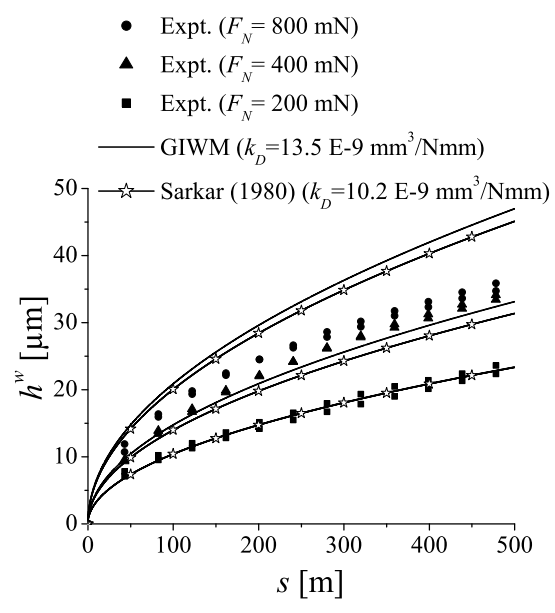




Figure 4

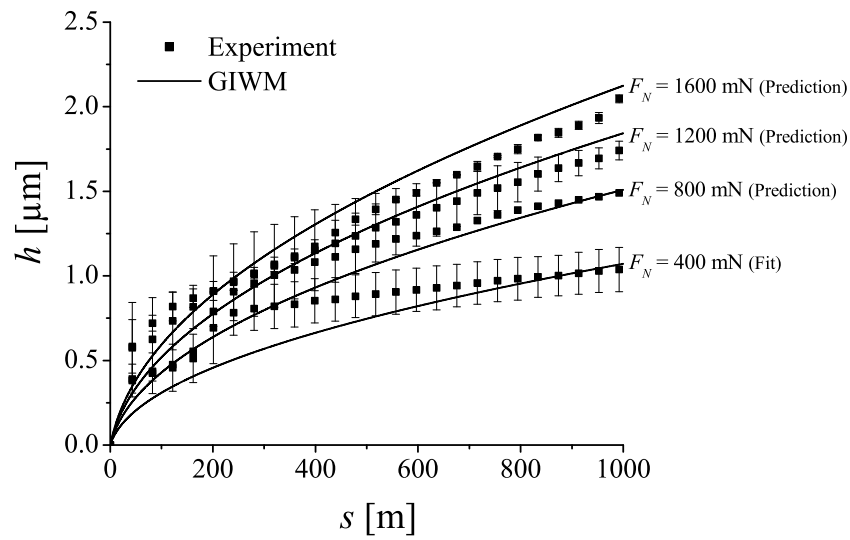


Figure 5a

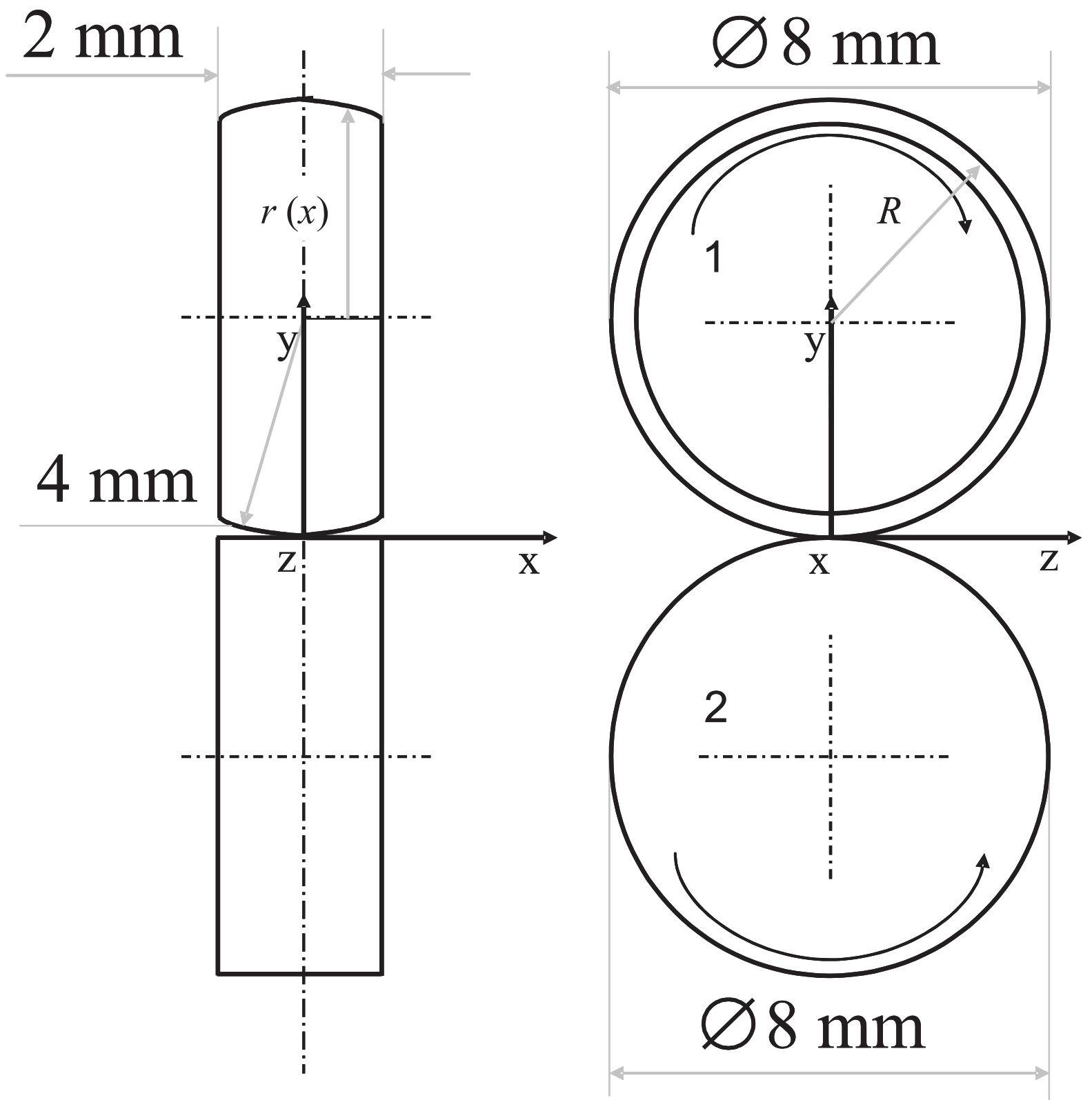
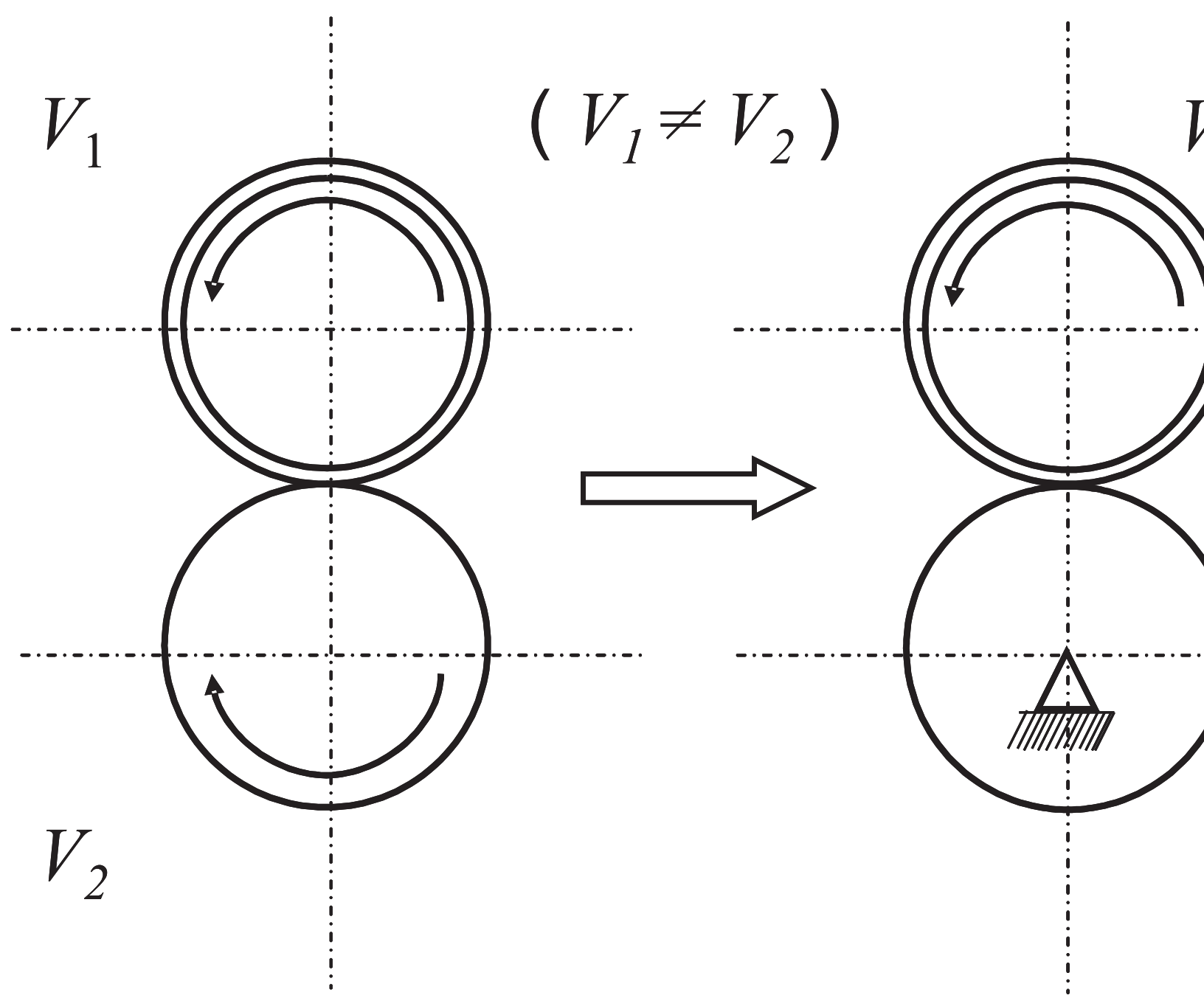


Figure 5b



**Figure 6**  
[Click here to download high resolution image](#)

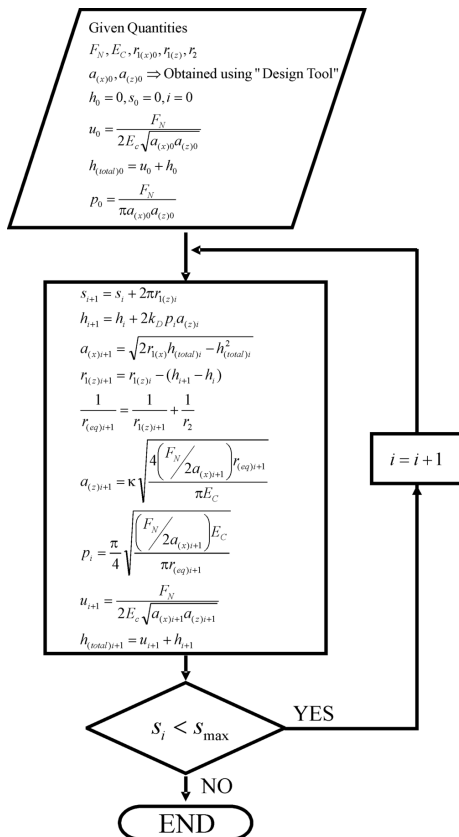


Figure 7a

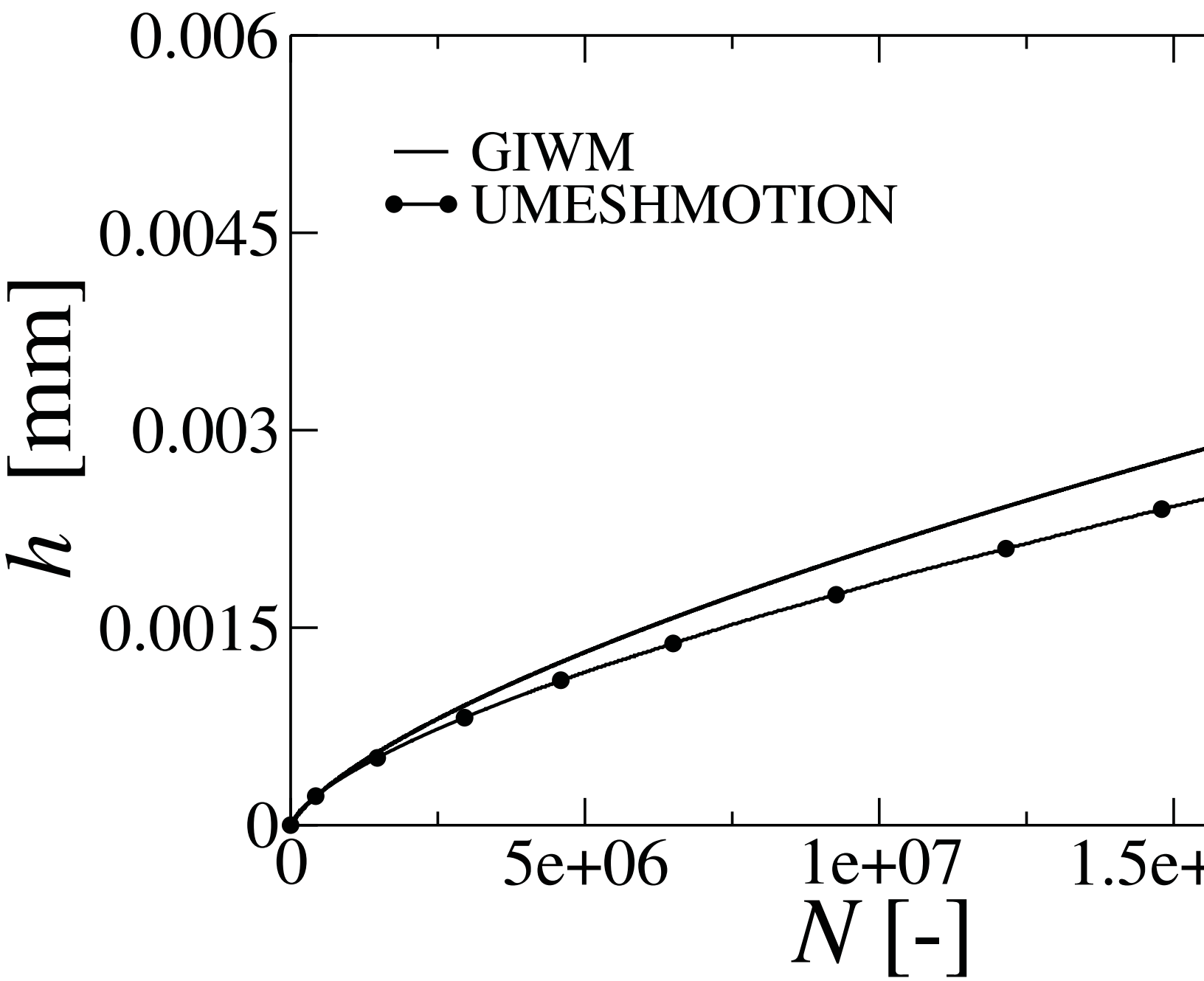


Figure 7b

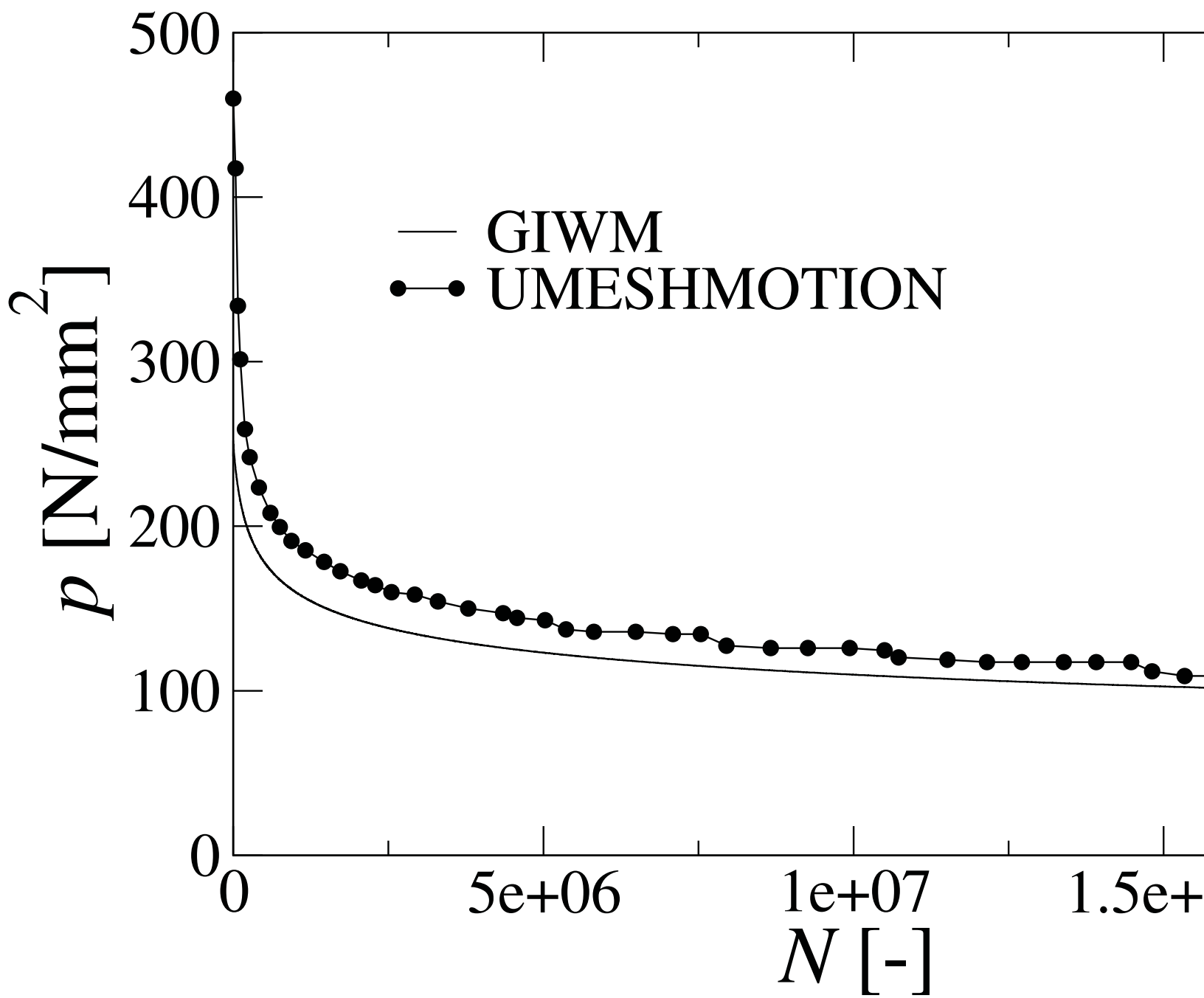


Figure 7c

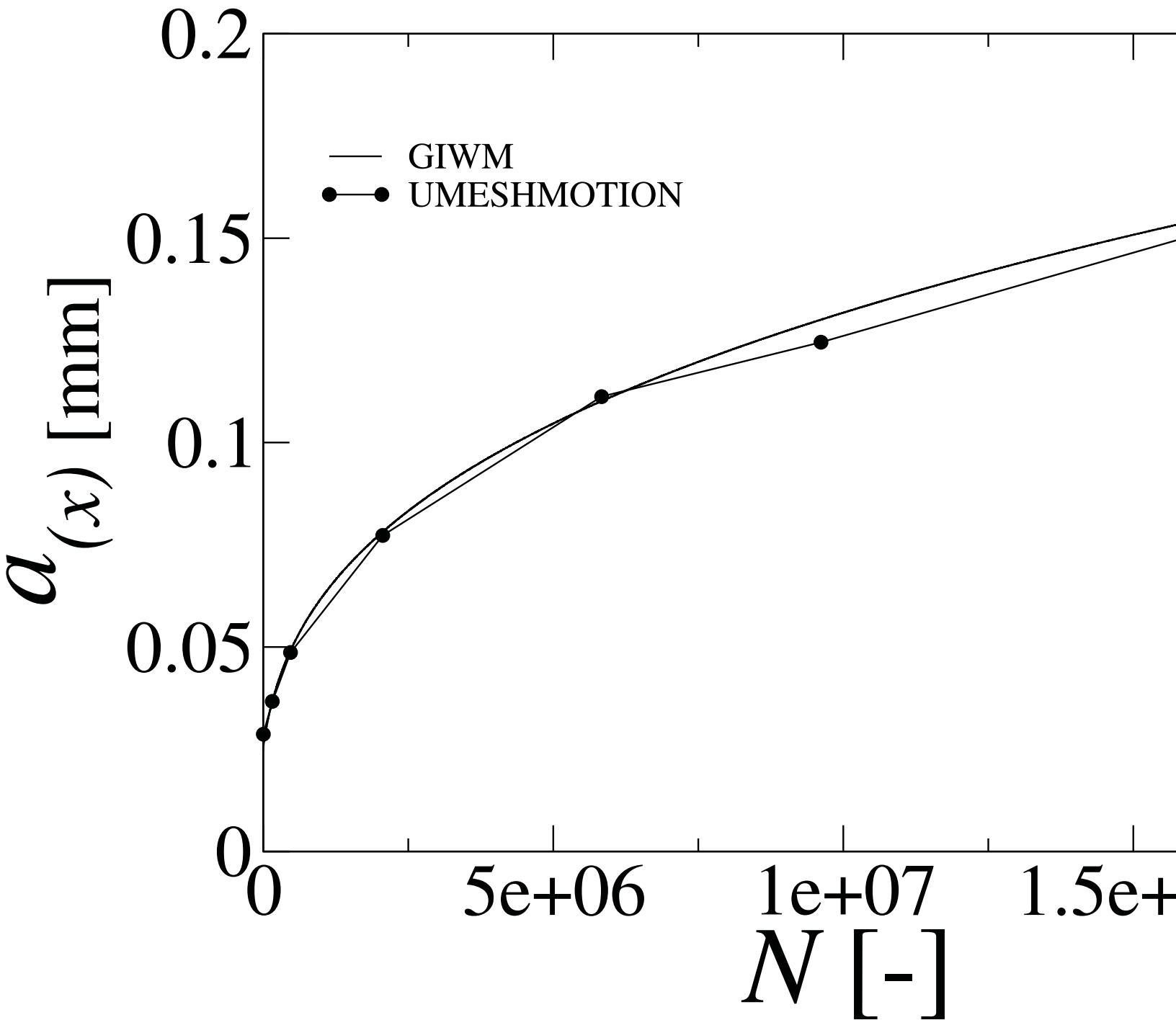


Figure 7d

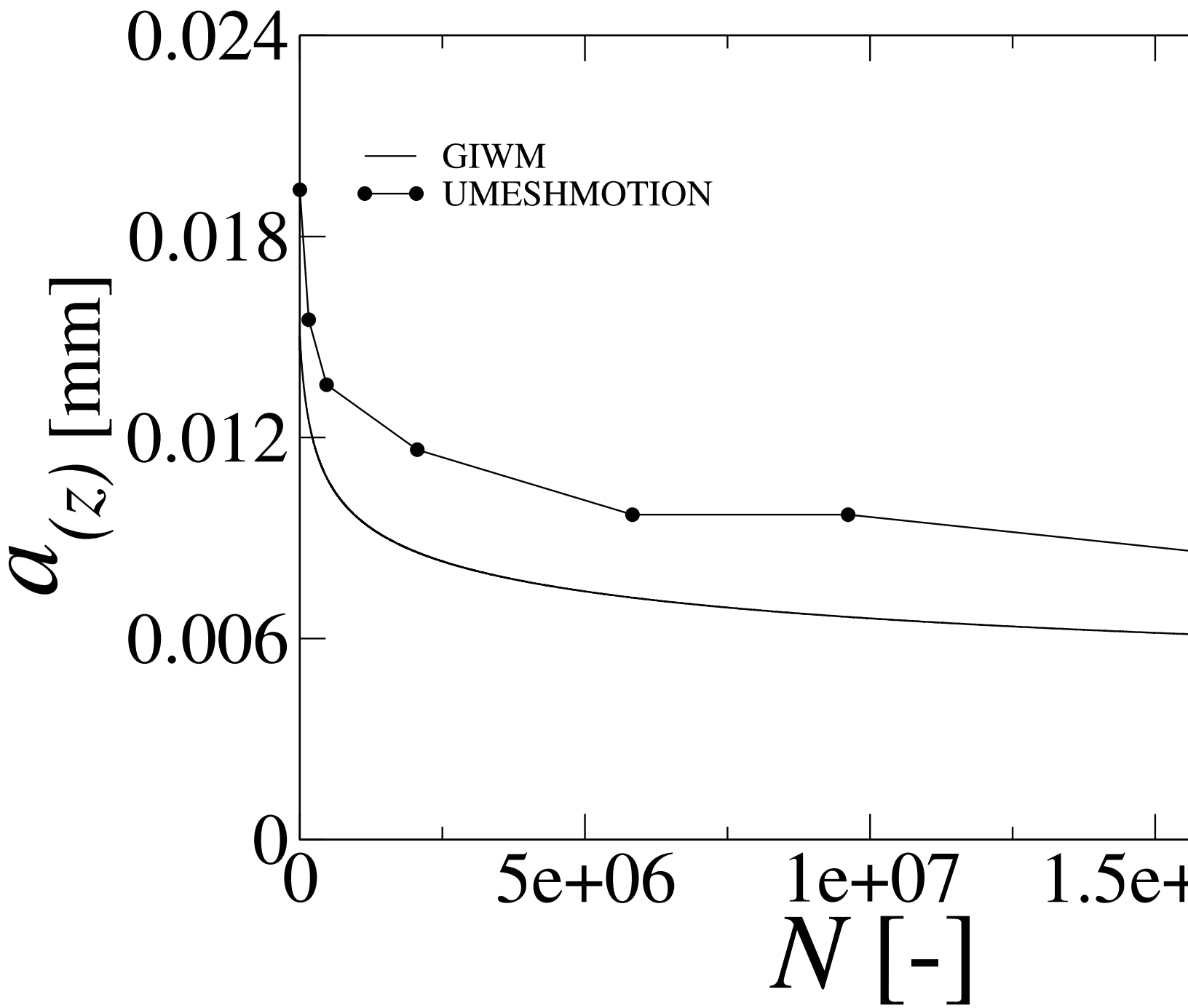




Figure 8

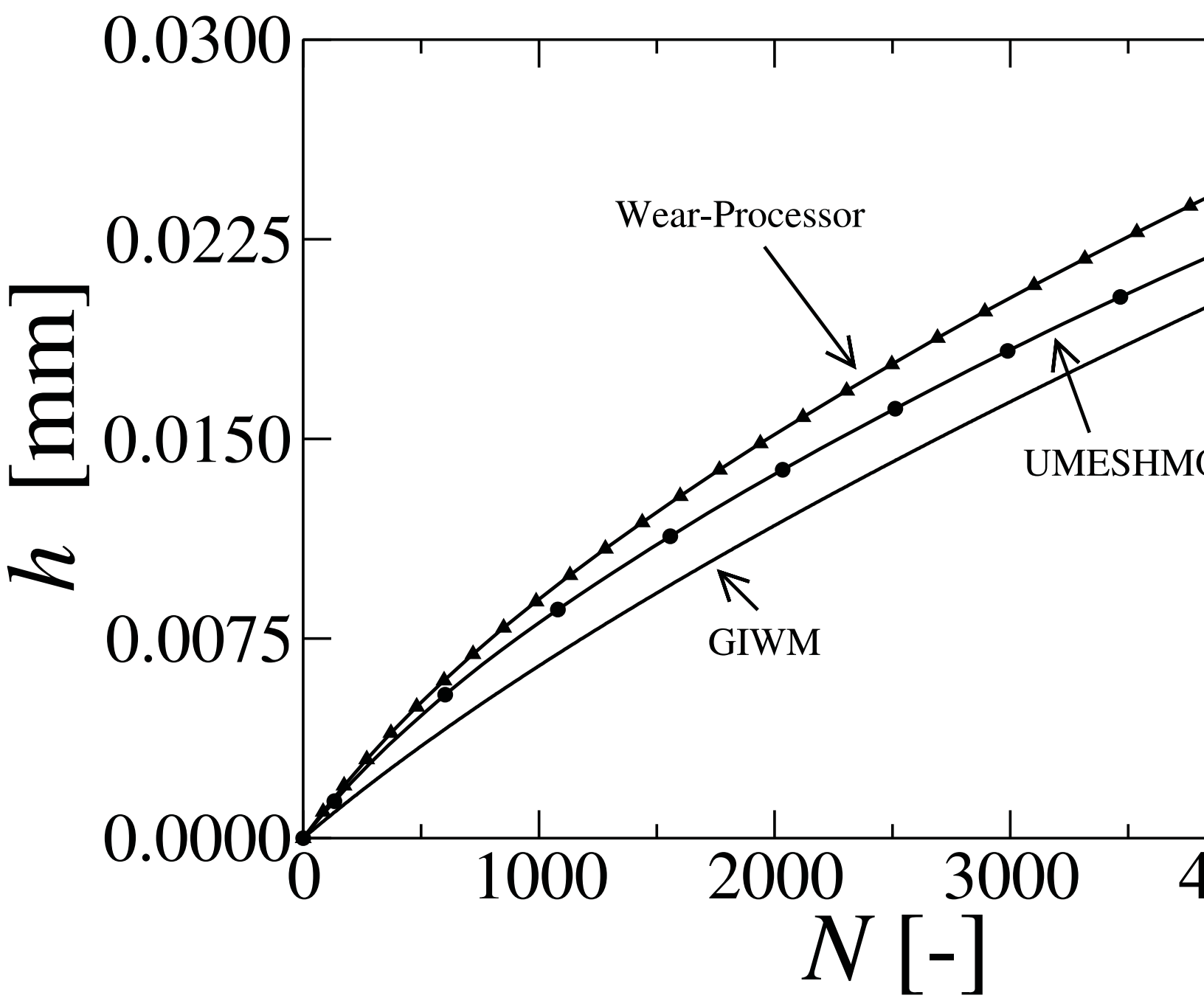


Figure 9a

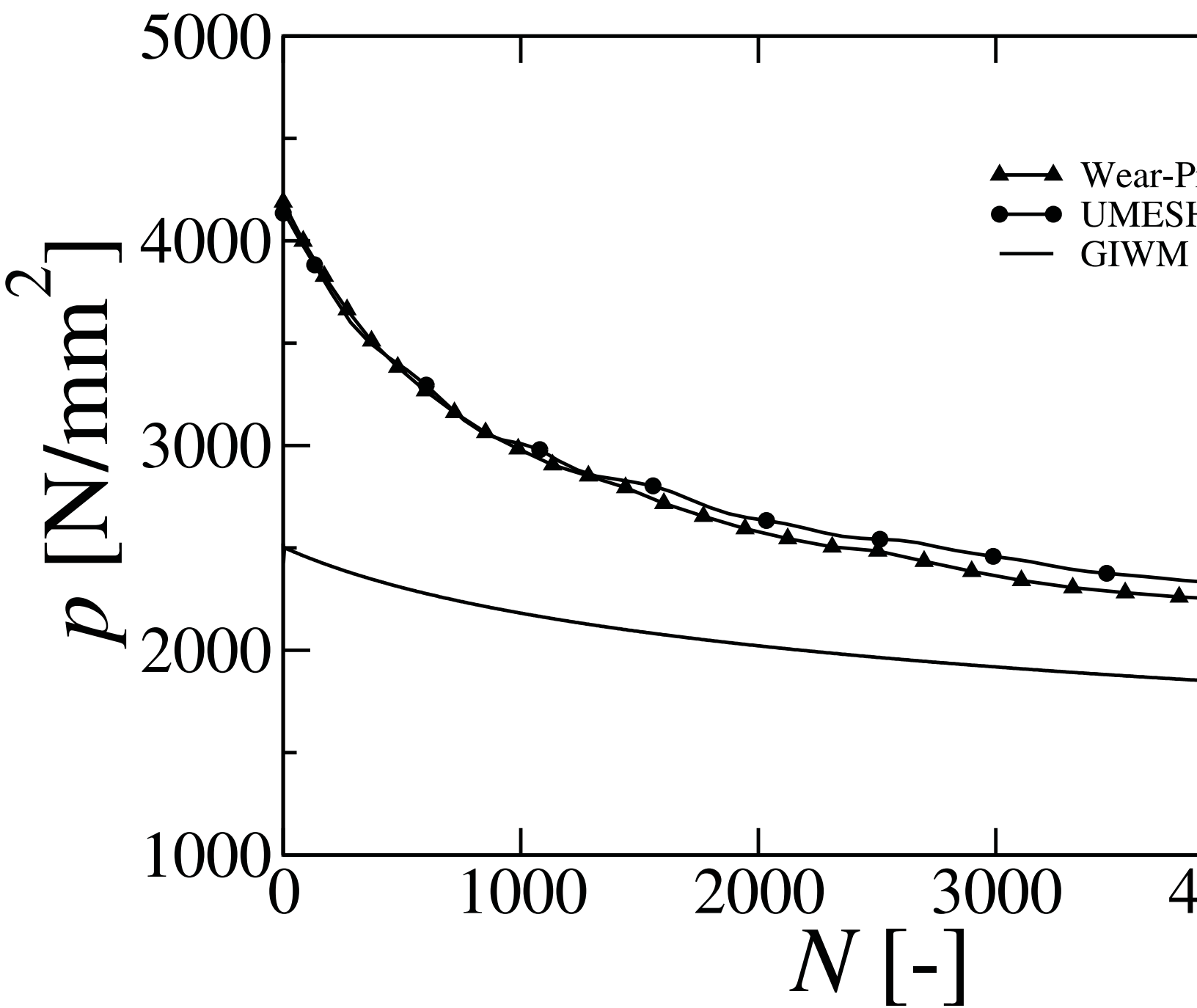


Figure 9b

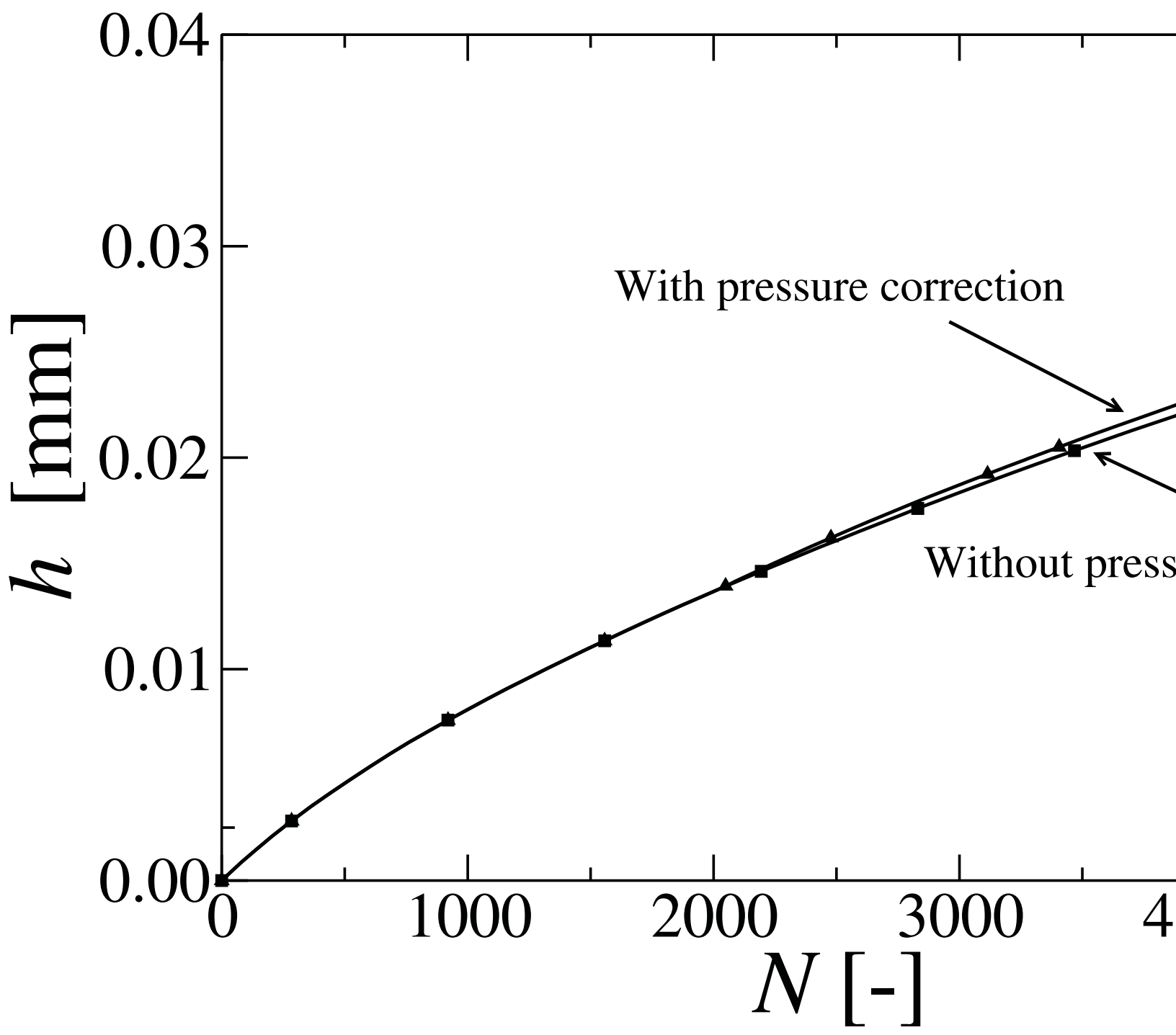


Table 1: Values of the parameters from the exponential fit (Equation 7) of the measured value of the friction coefficient as a function of the sliding distance for different normal loads

Parameter	200 mN	400 mN	800 mN
A	0.226	0.244	0.284
b	0.496	0.396	0.404
c	32.877	607.837	81.704

Table 2: Parameters used for the wear simulation using Wear-Processor and UMESHMOTION

Parameter	Value
Material	ZrO <sub>2</sub>
Young's Modulus	$E_t = E_b = 152 \text{ GPa}$
Poisson's Ratio	$\nu_t = \nu_b = 0.32$
Applied Normal Load	$F_N = 0.3 \text{ N}$
Friction Coefficient	$\mu = 0.6$
Dimensional Wear Coefficient	$k_D = 1 \times 10^{-10} \text{ mm}^3/\text{Nmm}$
Slip	10 %